Published in final edited form as:

Mol Cell. 2021 June 17; 81(12): 2625–2639.e5. doi:10.1016/j.molcel.2021.03.038.

Distinct PRC2 subunits regulate maintenance and establishment of *Polycomb* repression during differentiation

Ana Petracovici[1,2,3], **Roberto Bonasio**[2,3,*]

[1]Graduate Group in Cell and Molecular Biology, University of Pennsylvania Perelman School of Medicine, Philadelphia, PA, USA

[2]Epigenetics Institute, University of Pennsylvania Perelman School of Medicine, Philadelphia, PA, USA

[3]Department of Cell and Developmental Biology, University of Pennsylvania Perelman School of Medicine, Philadelphia, PA, USA

SUMMARY

The *Polycomb* repressive complex 2 (PRC2) is an essential epigenetic regulator that deposits repressive H3K27me3. PRC2 subunits form two holocomplexes—PRC2.1 and PRC2.2—but the roles of these two PRC2 assemblies during differentiation are unclear. We employed auxin-inducible degradation to deplete PRC2.1 subunit MTF2 or PRC2.2 subunit JARID2 during differentiation of embryonic stem cells (ESCs) to neural progenitors (NPCs). Depletion of either MTF2 or JARID2 resulted in incomplete differentiation due to defects in gene regulation. Distinct sets of *Polycomb* target genes were derepressed in absence of MTF2 or JARID2. MTF2-sensitive genes were marked by H3K27me3 in ESCs and remained silent during differentiation, whereas JARID2-sensitive genes were preferentially active in ESCs and became newly repressed in NPCs. Thus, MTF2 and JARID2 contribute non-redundantly to *Polycomb* silencing, suggesting that PRC2.1 and PRC2.2 have distinct functions in maintaining and establishing, respectively, *Polycomb* repression during differentiation.

eTOC blurb

Petracovici et. al employ inducible protein degradation to dissect the functions of subunits specific to the PRC2 holocomplexes PRC2.1 and PRC2.2 during differentiation. They uncover that PRC2.1 and PRC2.2 subunits regulate different gene sets with distinct chromatin and expression dynamics, suggesting underlying functional differences in maintaining and establishing *Polycomb* repression.

Graphical Abstract

*Lead contact, to whom correspondence should be addressed: roberto@bonasiolab.org.

AUTHOR CONTRIBUTIONS

A.P. and R.B. designed the study. A.P. performed all experiments and analyzed all data. A.P. and R.B. wrote the manuscript.

DECLARATION OF INTERESTS

The authors declare no competing interests.

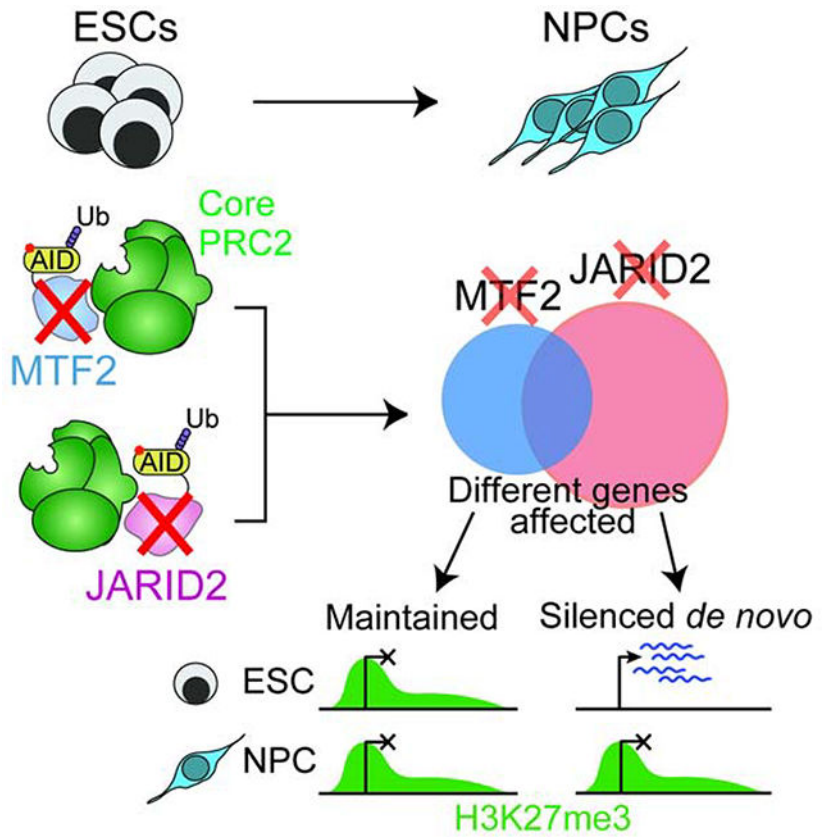

INTRODUCTION

Epigenetically inherited modifications of chromatin maintain transcriptional states across cell division, allowing for the establishment and propagation of different cell identities during development (Reinberg and Vales, 2018). A major effector of epigenetic silencing is the *Polycomb* repressive complex 2 (PRC2), an essential chromatin modifier that catalyzes mono-, di-, and trimethylation on lysine 27 of histone 3 (H3K27me1/2/3) (Laugesen et al., 2019; Yu et al., 2019). PRC2 is indispensable for embryogenesis (Faust et al., 1995; Grosswendt et al., 2020; O'Carroll et al., 2001; Pasini et al., 2004), and somatic mutations in its subunits are frequent in cancer (Comet et al., 2016). In humans, mutations in PRC2 cause Weaver syndrome, a developmental disorder characterized by abnormal tall stature, macrocephaly, and intellectual disability (Cooney et al., 2017; Gibson et al., 2012; Imagawa et al., 2018; Tatton-Brown et al., 2011).

H3K27me3 marks facultative heterochromatin, an epigenetically transmitted state of repressed chromatin that prevents the ectopic activation of genes not required in a given lineage (Bracken and Helin, 2009; Schuettengruber et al., 2017; Yu et al., 2019). Thus, the maintenance of H3K27me3 is key to the stability of transcriptional identities in the steady-state (Comet et al., 2016); however, during development different genes are marked by H3K27me3 in different lineages. Therefore, PRC2 must be able to establish new

H3K27me3-marked heterochromatic domains in addition to maintaining existing ones. The mechanisms that regulate this dual function of PRC2 are largely unknown.

PRC2 is composed of four core subunits: EZH2 [or its paralog EZH1 (Margueron et al., 2008)], which catalyzes H3K27me3 deposition; EED, which contains the H3K27me3-binding pocket that allows for epigenetic inheritance of the mark (Margueron et al., 2009); SUZ12, which functions as a scaffold (Chen et al., 2020; Chen et al., 2018; Hojfeldt et al., 2018); and the histone chaperone RbAp46/48 (Laugesen et al., 2019; Yu et al., 2019). Biochemical and proteomic analyses revealed that the PRC2 catalytic core assembles with mutually exclusive accessory subunits to form two distinct PRC2 holocomplexes: PRC2.1 and PRC2.2 (Chen et al., 2018; Hauri et al., 2016; Kloet et al., 2016). PRC2.1 is defined by the presence of a *Polycomb*-like protein (PCL1/PHF1, PCL2/MTF2, or PCL3/PHF19) and either EPOP or PALI1/2, while PRC2.2 is defined by the presence of two zinc-finger-containing subunits, AEBP2 and JARID2. PCL-containing and JARID2-containing PRC2 complexes are also present in *Drosophila melanogaster,* suggesting that they are a conserved feature of *Polycomb* function (Herz et al., 2012; Nekrasov et al., 2007).

In the last decade, the functions of different PRC2 subunits have been studied with a combination of knockout (KO), knockdown, biochemical, and structural analyses. The accessory subunits have been implicated in stimulating PRC2 catalytic activity *in vitro* and/or promoting PRC2 association with chromatin (Choi et al., 2017; Conway et al., 2018; Lee et al., 2018a; Li et al., 2010; Li et al., 2017; Sarma et al., 2008; Son et al., 2013; Zhang et al., 2011). PRC2.1 subunit MTF2—the predominant PCL in pluripotent cells (Kloet et al., 2016)—and its PHF1/PHF19 paralogs contain a Tudor domain that binds to transcription-associated H3K36me3, as well as a C-terminal winged-helix domain that binds CG-rich DNA (Ballare et al., 2012; Brien et al., 2012; Li et al., 2017; Perino et al., 2018). EPOP bridges PRC2 and the ElonginB/C proteins to fine-tune PRC2 activity at lowly-expressed genes (Beringer et al., 2016; Liefke et al., 2016), while the recently characterized PALI promotes PRC2 activity in pluripotent cells (Conway et al., 2018). PRC2.2 subunit JARID2 can be methylated by EZH2 resulting in a feedback stimulatory loop (Sanulli et al., 2015), and also contains a binding pocket for PRC1-deposited H2AK119ub1, suggesting a function in mediating PRC2 recruitment to chromatin regions marked by *Polycomb* repressive complex 1 (PRC1) (Cooper et al., 2016; Healy et al., 2019; Kalb et al., 2014; Kasinath et al., 2021).

A central unanswered question is whether PRC2.1 and PRC2.2 are functionally redundant, or whether they play mechanistically distinct roles in regulating PRC2 activity. Two recent studies addressed this by using genetic KOs to dissect the functions of individual accessory subunits of PRC2 in mouse embryonic stem cells (ESCs), and came to the conclusion that PRC2.1 and PRC2.2 are largely redundant in the pluripotent state (Healy et al., 2019; Hojfeldt et al., 2019). By contrast, genetic evidence in mice indicates that subunits from both complexes are needed for proper development (Duncan, 1982; Motoyama et al., 1997; Rothberg et al., 2018; Takeuchi et al., 1999; Takeuchi et al., 1995), although the mechanistic bases for this requirement are not known. These observations suggest that the distinct functions of the accessory subunits of PRC2.1 and PRC2.2 might be revealed by selectively depleting them during cell fate transitions.

In the current study, we implement auxin-inducible degradation to acutely deplete subunits specific to PRC2.1 and PRC2.2 during the differentiation of ESCs to neural progenitors (NPCs). We demonstrate that PRC2.1 subunit MTF2 and PRC2.2 subunit JARID2 are independently required for the repression of distinct subsets of PRC2 target genes during neural differentiation. Genes specifically sensitive to loss of MTF2 or JARID2 exhibited different expression dynamics and chromatin properties, suggesting a mechanistic difference between PRC2.1 and PRC2.2 in mediating the maintenance *vs.* establishment of *Polycomb*-mediated repression.

RESULTS

Acute and selective depletion of PRC2 subunits with auxin-induced degradation

To compare the effects of disrupting PRC2.1 or PRC2.2 function in the same experimental system, we inserted an auxin-inducible degron (AID) fusion tag at the endogenous loci encoding the core subunit SUZ12 (all of PRC2), MTF2 (PRC2.1-specific), or JARID2 (PRC2.2-specific) in ESCs. These cell lines will hereafter be referred to as SUZ12-AID, MTF2-AID, and AID-JARID2, respectively (Fig. 1A). These cells also express a transgene for the F-box protein osTIR1 from the *TIGRE* locus (Zeng et al., 2008), allowing for the rapid ubiquitination and proteasomal degradation of AID-tagged proteins in presence of the plant auxin indole-3-acetic acid (Nishimura et al., 2009) (Fig. 1A). Homozygous clones for the AID fusion tag insertion were identified by western blot and validated by Sanger sequencing. Co-immunoprecipitation experiments in the tagged lines showed that the AID fusion did not prevent the incorporation of tagged subunits into PRC2 (Fig. S1A). The engineered ESC lines expressed pluripotency markers at normal levels and exhibited morphology indistinguishable from that of the untagged parental line (Fig. S1B–C).

Addition of auxin resulted in rapid and substantial degradation of the tagged subunits (Fig. 1B), with maximal depletion apparent by 2 hours in all cell lines. The degradation was specific to the tagged subunit in each cell line, as JARID2 and MTF2 levels were unaffected upon depletion of the reciprocal subunit. Depletion of core PRC2 subunit SUZ12 led to substantial reduction in bulk H3K27me3 levels 24 hours after auxin treatment, whereas total H3K27me3 levels in ESCs were unaffected by MTF2 or JARID2 depletion (Fig. 1B), despite the near-complete loss of the depleted PRC2 subunits from chromatin (Fig. S1D–E).

RNA-seq following a 12-hour depletion of SUZ12 resulted in the deregulation of several hundred genes (Fig. 1C, left), which were almost exclusively upregulated, in line with the function of PRC2 as an epigenetic repressor. The majority of deregulated genes were PRC2 targets, as defined by profiling genome-wide occupancy of SUZ12 by CUT&RUN (see STAR Methods), indicating that at this early time point of depletion, direct targets of PRC2 repression are preferentially affected ($P < 10^{-15}$, Fisher test). In contrast, the gene expression changes following depletion of JARID2 or MTF2 in ESCs were modest, which was consistent with previous observations that these two accessory subunits perform largely redundant functions in steady-state pluripotent ESCs (Healy et al., 2019; Hojfeldt et al., 2019). Auxin treatment of the parental ESCs that express *TIR1* but carry unmodified *Suz12, Mtf2,* and *Jarid2* alleles (henceforth referred to as “WT” cells) resulted in virtually no gene deregulation (Fig. S1F).

Core PRC2 is required for NPC differentiation

To study the consequences of acute PRC2 depletion during the process of differentiation and lineage commitment, we differentiated ESCs into NPCs by adding basic fibroblast growth factor (bFGF) for 72 hours, followed by smoothened agonist (SAG) for 48 hours (Fig. 2A, left) (Cruz-Molina et al., 2017; Gouti et al., 2014). Differentiation of the WT ESCs resulted in characteristic morphological changes by day 5, including the formation of spiny processes typical of NPCs (Martinez-Cerdeno and Noctor, 2018) (Fig. 2A, right). By day 5, the cells had upregulated genes associated with NPC identity—including *Nestin, Fabp7,* and *Sox1* (Bertrand et al., 2002; Gouti et al., 2014; Lendahl et al., 1990; Wood and Episkopou, 1999) —and downregulated pluripotency genes such as *Klf4, Nanog,* and *Pou5f1/Oct4* (Fig 2B, yellow dots). In absence of auxin, ESCs expressing AID-tagged SUZ12, MTF2, or JARID2 differentiated to NPCs with comparable efficiency to that of WT cells (Fig. S2A–B), demonstrating that the AID fusion did not compromise the function of these PRC2 subunits in the context of neural differentiation.

Consistent with the requirement for PRC2 in the early stages of development (Faust et al., 1995; O'Carroll et al., 2001; Pasini et al., 2004), depletion of SUZ12—which completely abolishes functional PRC2—was incompatible with NPC differentiation, as demonstrated by severe morphological defects of SUZ12-depleted cells on day 5, whereby cells remained small and flattened and failed to develop neural processes characteristic of NPCs (Martinez-Cerdeno and Noctor, 2018) (Fig. 2C). RNA-seq of SUZ12-depleted cells on day 5 revealed that over 5,500 genes were differentially expressed (FDR < 10% and fold-change > 1.5), indicating massive defects in transcriptional regulation (Fig. 2D). SUZ12-deficient cells failed to upregulate known NPC-associated genes including *Nestin, Fabp7* and *Sox1* (Fig. 2D, yellow dots). As a control, differentiation of WT ESCs into NPCs proceeded unimpeded by the presence of auxin and led to no significant gene deregulation (Fig. S2C), confirming that the differentiation defects observed upon auxin treatment of SUZ12-AID cells were due to loss of PRC2 function.

PRC2 acts to repress genes from alternate lineages during differentiation (Schuettengruber et al., 2017). Accordingly, genes normally downregulated in the transition from ESCs to NPCs (Fig. 2B, blue dots) were disproportionately affected and failed to be silenced in absence of PRC2 (Fig. 2E, blue dots). These included pluripotency markers *Klf4, Nanog,* and *Pou5f1/Oct4* (Fig. 2E, yellow dots), indicating a general failure in exiting pluripotency. Direct PRC2 targets (Fig. 2D, light green dots) that were not properly repressed in SUZ12-deficient cells were enriched for GO-terms associated with transcriptional regulation and embryonic development (Fig. 2F), consistent with the known role of PRC2 in repressing developmentally important transcription factors (Boyer et al., 2006).

In conclusion, acute depletion of the core PRC2 subunit SUZ12 (present in both PRC2.1 and PRC2.2) prevents the acquisition of NPC identity by extensive disruption of *Polycomb*-mediated gene silencing during differentiation.

MTF2 and JARID2 are independently required for the transcriptional identity of NPCs

While recent studies have suggested that PRC2.1 and PRC2.2 are redundant in the pluripotent state (Healy et al., 2019; Hojfeldt et al., 2019), whether or not this redundancy extends to lineage commitment and differentiation has not been investigated. Furthermore, whether MTF2 (PRC2.1) and JARID2 (PRC2.2) have different molecular functions in differentiated cells is unknown.

To interrogate the roles of MTF2 and JARID2 during differentiation, we used AID to degrade MTF2 or JARID2 in ESCs, followed by NPC differentiation in the presence of auxin (Fig. 3A–B, left). RNA-seq on day 5 of differentiation revealed the dysregulation of 424 and 1,792 genes following MTF2 and JARID2 depletion, respectively (Fig. 3A–B, right). This result indicates that MTF2 and JARID2 are both required for proper gene regulation during NPC differentiation, and suggests that the PRC2.1 and PRC2.2 might play functionally distinct roles in *Polycomb* silencing. Similar to the depletion of all PRC2 (Fig. 2E), genes that were specifically downregulated during the ESC to NPC transition in WT cells (Fig. 2B, blue dots) showed impaired silencing in the absence of MTF2 or JARID2, and the extent of this bias was more pronounced in JARID2-depleted cells than in MTF2-depleted cells (Fig. 3C–D, blue dots).

Furthermore, MTF2-depleted and JARID2-depleted cells failed to properly upregulate several genes associated with neural identity (Martinez-Cerdeno and Noctor, 2018; Wood and Episkopou, 1999) (Fig. 3E), indicating a reduced capacity to acquire the transcriptional state of NPCs. Since addition of SAG in our protocol induces NPC ventralization, we also analyzed the expression of genes associated with ventral regional identity (Gouti et al., 2014). Both MTF2 and JARID2 depletion impaired the full induction of ventral identity genes, although the effects were more pronounced in the JARID2 depletion (Fig. S3A).

Altogether, the observed gene expression defects indicate that both MTF2 and JARID2 are independently required for proper gene regulation during NPC differentiation.

MTF2 and JARID2 repress distinct gene sets during NPC differentiation

The genome-wide distributions of MTF2 and JARID2 in ESCs overlap and it has been argued that they interchangeably contribute to *Polycomb* silencing at the same set of genes (Healy et al., 2019; Hojfeldt et al., 2019). Given the gene expression defects observed upon MTF2 or JARID2 depletion during NPC differentiation, we wondered whether the genes affected were different.

An analysis of the genes differentially expressed on day 5 of differentiation following SUZ12, MTF2, or JARID2 depletion revealed a substantial overlap in the genes affected by SUZ12 depletion and those deregulated upon MTF2 or JARID2 depletion (90% and 91%, respectively), confirming that the gene deregulation caused by MTF2 or JARID2 depletion was due to perturbing PRC2 function (Fig. 4A, top). However, a considerable number of genes were uniquely sensitive to loss of MTF2 or JARID2 but not to the depletion of the reciprocal subunit. Specifically, we detected 1,534 genes that were deregulated uniquely following JARID2 depletion, and 166 genes that were only sensitive to MTF2 depletion (Fig. 4A, top).

To exclude the possibility of secondary effects from indirectly regulated genes, we repeated this analysis exclusively on PRC2 targets (as defined by SUZ12 occupancy, see STAR Methods) that were upregulated upon depletion of SUZ12, MTF2 or JARID2. This analysis revealed an even more striking divergence in the effects of depleting MTF2 or JARID2, with approximately 60% of genes deregulated following MTF2 depletion and 80% genes deregulated following JARID2 depletion only affected by the loss of the respective subunit (Fig. 4A, bottom). Analysis of the expression patterns of these PRC2 targets that responded differentially to MTF2-or JARID2 depletion allowed us to define two stringent sets of genes that were significantly derepressed upon loss of MTF2 or JARID2, were unaffected by the loss of the reciprocal subunit, and had comparable basal expression across cell lines in control conditions (Fig. 4B–C). These refined sets of subunit-specific upregulated PRC2 targets are used for all subsequent analyses and will be referred to as MTF2-specific and JARID2-specific, respectively. The differential sensitivity of PRC2 targets to depletion of PRC2.1 or PRC2.2 was validated on a subset of genes in an independent experiment using RT-qPCR (Fig. 4D).

GO analyses revealed that the MTF2-specific genes defined above were enriched for functional terms associated with cardiovascular development (Fig. S3B), whereas JARID2-specific genes were enriched for a broader set of developmental terms, including epithelium morphogenesis and transcriptional regulation (Fig. S3C), suggesting that MTF2-specific and JARID2-specific genes represent functionally distinct sets.

To gain insight into the chromatin changes that might accompany the gene expression effects observed above, we differentiated MTF2-AID and AID-JARID2 ESCs in the presence of auxin and performed CUT&RUN for H3K27me3 and for the transcription-associated H3K4me3 mark. Depletion of MTF2 or JARID2 caused a modest decrease in H3K27me3 across all PRC2 targets in NPCs (Fig. S4A), consistent with their roles as stimulators of PRC2 activity (Choi et al., 2017; Lee et al., 2018a; Li et al., 2010; Sarma et al., 2008; Son et al., 2013; Zhang et al., 2011). However, upon further inspection, MTF2-specific genes showed a more pronounced loss of H3K27me3 in auxin-treated MTF2-AID NPCs, whereas JARID2-specific genes lost relatively more H3K27me3 in auxin-treated AID-JARID2 NPCs (Fig. S4B). We observed opposite trends in H3K4me3, for which MTF2-specific and JARID2-specific genes showed more pronounced increases in the respective subunit depletions (Fig. S4C–D).

Taken together, our results suggest that MTF2 and JARID2 repress different sets of genes, potentially with distinct developmental functions, during differentiation.

The genomic distributions of MTF2 and JARID2 overlap in NPCs

To investigate the reason for the differential sensitivities of MTF2- and JARID2-specific genes to the depletion of the respective PRC2 subunit, we compared the chromatin states of these two gene sets during the differentiation of WT cells without perturbations in PRC2 function. First, we compared the distribution of MTF2 and JARID2 themselves. PRC2.1 and PRC2.2 are known to colocalize on chromatin in ESCs (Healy et al., 2019; Hojfeldt et al., 2019), but their genomic distributions might diverge in differentiated cells, thus explaining the unique sensitivity of MTF2- and JARID2-specific genes. However, CUT&RUN in WT

NPCs revealed an extensive overlap in the chromatin occupancy of MTF2 and JARID2, which, as expected, also coincided with the distribution of the core subunit SUZ12 (Fig. 5A, Fig. S5A).

A more quantitative comparison of MTF2 and JARID2 occupancy at the transcription start site (TSS) of MTF2-specific or JARID2-specific derepressed genes also failed to reveal substantial differences (Fig. S5B). Although we cannot conclude that PRC2.1 and PRC2.2 bind simultaneously to PRC2 target genes in individual cells, these data indicate that, at the population level, PRC2.1 and PRC2.2 bind with comparable frequencies to all targets, suggesting that differences in binding of MTF2 or JARID2 cannot explain the existence of distinct MTF2- and JARID2-sensitive genes.

MTF2-specific genes are heavily marked by H3K27me3 in ESCs and NPCs and have high CpG densities

We reasoned that underlying differences in histone modifications at these genes might be responsible for differential sensitivity of certain genes to MTF2 or JARD2 depletion. We performed CUT&RUN in WT ESCs and NPCs to compare the density of H3K27me3 and H3K4me3 at the promoters of MTF2-specific and JARID2-specific genes and analyzed their dynamics during WT NPC differentiation. Both MTF2- and JARID2-specific genes were enriched for the co-occurrence of H3K27me3 and H3K4me3 at the NPC stage (Fig. S5C), consistent with previous studies showing that genes with “bivalent” promoters are more sensitive to the loss of *Polycomb* repression (Jadhav et al., 2016). However, when we compared the relative abundance of H3K27me3 and H3K4me3, it became apparent that MTF2-specific and JARID2-specific genes displayed different chromatin dynamics during differentiation. Promoters of MTF2-specific genes had higher H3K27me3 density and SUZ12 occupancy than JARID2-specific genes in ESCs and this difference decreased in NPCs (Fig. 5B). When compared to the set of all PRC2 targets, MTF2-specific genes also exhibited higher SUZ12 and H3K27me3 at their TSS (Fig. S5D). Conversely, JARID2-specific genes exhibited higher H3K4me3 at their TSS at the ESC stage, which decreased upon differentiation to NPCs (Fig. 5B).

MTF2 contains a winged-helix domain that binds to CG-rich DNA *in vitro,* and studies have implicated MTF2 in recruiting PRC2 to CpG-rich regions in ESCs (Li et al., 2017; Perino et al., 2018). To investigate whether MTF2 may preferentially regulate genes with higher CpG densities, we compared the CpG density at the promoter regions of MTF2-specific and JARID2-specific genes. The promoters of MTF2-specific genes had significantly greater CpG densities than those of JARID2-specific genes, as well as the set of all of PRC2 targets in our system (Fig. S5E). Combined with the results of our chromatin analyses above, this suggests that MTF2 is required to maintain the repression of PRC2 target genes with high CpG densities at their promoters and that are marked by H3K27me3 both before and after differentiation.

JARID2-specific genes are silenced *de novo* during the ESC–NPC transition

Based on the observation that JARID2-specific genes were relatively depleted for H3K27me3 and enriched for H3K4me3 before differentiation (Fig. 5B), we hypothesized

that these genes might be transcriptionally active in ESCs. Consistent with a positive correlation between H3K4me3 levels and transcriptional activity (Howe et al., 2017), JARID2-specific genes were expressed at higher levels in ESCs compared to both MTF2-specific genes and all PRC2 target genes (Fig. 5C, Fig. S5D). The majority of these JARID2-specific genes started as transcriptionally active in ESCs and became subsequently downregulated at the NPC stage, indicating that they preferentially acquire *Polycomb* repression over the course of differentiation (Fig. 5D). In contrast, virtually all MTF2-specific genes remained lowly expressed in both ESCs and NPCs, suggesting that they are constitutive *Polycomb* targets whose repression is maintained by PRC2 as the cells differentiate (Fig. 5D). This is consistent with the high levels of both H3K27me3 and SUZ12 we observed at the TSS of MTF2-specific genes in ESCs and NPCs (Fig. 5B, Fig. S5D).

Examination of the chromatin state of individual MTF2-specific and JARID2-specific genes further supported our conclusions above (Fig. 5E, red and green tracks). MTF2-specific genes exhibited higher H3K27me3 levels at their TSS than JARID2-specific genes, and this H3K27me3 pattern was maintained across differentiation to NPCs (Fig. 5E, top; Fig. S5F, left). In agreement with their lower expression levels, MTF2-specific genes also had less H3K4me3 at their TSS in ESCs compared to JARID2-specific genes. Conversely, when we examined individual JARID2-specific genes that become silenced during differentiation, we noticed that these genes tended to start with low H3K27me3 and relatively high H3K4me3 in ESCs, then gained H3K27me3 with a concomitant loss of H3K4me3 in NPCs (Fig. 5E, bottom; Fig. S5F, right).

To extend our conclusions to an additional lineage, we depleted SUZ12, MTF2, or JARID2 in the AID-tagged lines during differentiation to a cardiac precursor (CP) fate (Fig. S6A–B) (Oh and Ishikawa, 2018; Wamstad et al., 2012) and analyzed the resulting effects on gene expression by RNA-seq (Fig. S6C–E). Once again, MTF2 and JARID2 depletion affected non-overlapping subsets of PRC2 targets, albeit with a smaller number of genes affected by MTF2 depletion compared to the effects in NPCs (Fig. S6F). Analysis of the expression dynamics and chromatin states of these MTF2-specific and JARID2-specific genes confirmed that MTF2-specific genes had low expression in both ESCs and differentiated CPs, whereas JARID2-specific genes started as highly expressed in ESCs, with correspondingly high H3K4me3 levels, and tended to become silenced *de novo* during differentiation to CPs (Fig. S6G–I).

Together, analyses in two distinct differentiation paradigms support the conclusion that JARID2 is specifically required for the establishment of *Polycomb* repression on subsets of genes that are transcriptionally active in ESCs and must be silenced upon acquisition of new cell identities during differentiation.

Genes silenced by JARID2 *de novo* are pre-marked by H2AK119ub in ESCs

The observed chromatin and expression dynamics at JARID2-specific genes during differentiation prompted us to investigate the mechanism by which JARID2 might mediate *de novo* silencing of its target genes. JARID2 contains a ubiquitin interaction motif (UIM) that binds to H2AK119ub1 deposited by variant PRC1 complexes (Cooper et al., 2016; Kalb

et al., 2014), suggesting a potential role in mediating PRC2 recruitment to regions previously marked by PRC1. Furthermore, interactions between the JARID2 UIM domain and H2AK119ub1 result in stimulation of PRC2 activity *in vitro* (Kasinath et al., 2021). This led us to wonder whether genes specifically regulated by JARID2 in our system—which undergo *de novo* silencing upon differentiation—might be "pre-marked" by H2AK119ub1 in ESCs, and thus require the presence of JARID2 to mediate efficient binding of PRC2 and subsequent deposition of H3K27me3.

Indeed, JARID2-specific and MTF2-specific genes exhibited similar levels of H2AK119ub1 at their TSS in ESCs (Fig. 5F, left; Fig. S5G), despite their strikingly different expression profiles (Fig. 5C) and H3K27me3 levels (Fig. 5B). H2AK119ub1 levels at JARID2-specifc and MTF2-specific genes were higher than the average across all genes (Fig. 5F), demonstrating a true enrichment that persisted upon differentiation to NPCs (Fig. 5F, right). Inspection of H2AK119ub1 at individual JARID2-specific and MTF2-specific genes (Fig. 5E; Fig. S5F, purple tracks) validated our genome-wide analyses and confirmed that JARID2-specific genes are marked by H2AK119ub1 in ESCs despite their transcriptionally active state.

DISCUSSION

We interrogated the roles of PRC2.1 subunit MTF2 and PRC2.2 subunit JARID2 during directed differentiation to the neural lineage using auxin-inducible degradation. Acute depletion of MTF2 or JARID2 resulted in the deregulation of hundreds of genes during the differentiation of ESCs to neural progenitors, indicating that both subunits are independently required for proper gene regulation during this cell identity transition. While JARID2 and MTF2 were redundant for the proper regulation of many PRC2 targets, a small but considerable number of genes were uniquely sensitive to depletion of one or the other accessory subunit. These distinct and unique targets for MTF2 and JARID2 activity displayed different transcriptional and chromatin dynamics across differentiation, revealing unexpected functional differences between individual subunits comprising PRC2.1 and PRC2.2.

PRC2.1 and PRC2.2, redundant or distinct?

Recent studies in ESCs have suggested that PRC2.1 and PRC2.2 are redundant in the pluripotent state. Both MTF2 and JARID2 can effectively restore *Polycomb* silencing patterns in ESCs after erasure of the H3K27me3 mark (Oksuz et al., 2018) and single KO of *Mtf2* or *Jarid2* does not substantially affect gene expression in ESCs (Healy et al., 2019; Hojfeldt et al., 2019). Our own acute depletion experiments using AID confirmed these previous findings, showing that acute depletion of MTF2 or JARID2 does not affect the gene expression profile in pluripotent ESCs at steady-state, whereas depletion of SUZ12 resulted in derepression of a subset of PRC2 targets as early as 12 hours after auxin treatment (Fig. 1). Thus, the apparent redundancy of PRC2.1 and PRC2.2 in ESCs is not due to the lack of temporal resolution of genetic approaches, but rather appears to be an inherent feature of PRC2 function in pluripotent cells.

There is a large subset of PRC2 target genes whose expression is unaffected by depletion of either MTF2 or JARID2, although their silencing still requires core PRC2 subunit SUZ12 (Fig. 4A). At these genes, the function of MTF2 and JARID2 may be interchangeable for proper *Polycomb* repression, or may not be required at all, given that combined KO of *Jarid2* and all *Pcl1/2/3* in ESCs results in a 4-fold lower transcriptional effect compared to KO of core subunit SUZ12 (Hojfeldt et al., 2019). At these loci the PRC2 core alone may be capable of maintaining H3K27me3 levels sufficient for repression, possibly via its read-write mechanism (Hansen et al., 2008; Margueron et al., 2009; Reinberg and Vales, 2018) (Fig. 6A). However, acute depletion of only MTF2 or only JARID2 during differentiation resulted in the deregulation of a considerable number of genes, the majority of which did not overlap (Fig. 4), suggesting that certain chromatin contexts require the specific action of MTF2-containing PRC2.1 or JARID2-containing PRC2.2. Still, we cannot exclude the possibility that some genes require the function of PRC2.1 or PRC2.2 accessory subunits other than MTF2 or JARID2, which we have not investigated in this study. In line with this notion, the smaller number of genes affected by MTF2 *vs.* JARID2 depletion might be explained by the presence of MTF2 paralogs PHF1 and PHF19, which we did not target for degradation and are known to be upregulated during differentiation (Kloet et al., 2016; Oliviero et al., 2016; Walker et al., 2010).

Requirement for MTF2 and JARID2 in differentiation and development

In vivo, Mtf2 and *Jarid2* are expressed in a wide range of developing and adult tissues, albeit with different relative abundances (Petryszak et al., 2016; Walker et al., 2010). MTF2 and JARID2 may therefore be involved in regulating PRC2 for proper cell identity specification in multiple organs, as evidenced by the distinct lethal phenotypes of null alleles of these subunits. *Mtf2* KO embryos exhibit severe anemia, hemorrhage, and growth abnormalities (Rothberg et al., 2018), while brain, heart, spleen, and liver defects are observed in *Jarid2* KO embryos (Motoyama et al., 1997; Takahashi et al., 2004; Takeuchi et al., 1999; Takeuchi et al., 1995).

How can MTF2 and JARID2 be redundant in ESCs and yet independently required in development? Using an *in vitro* differentiation system and AID-induced acute depletion, we were able to reconcile these findings. Although acute depletion of MTF2 or JARID2 in ESCs did not have an impact on their transcriptional state (Fig. 1), both accessory subunits were necessary for the cells to acquire the transcriptional identity of lineage-committed NPCs (Fig. 3). Furthermore, our results suggest a mechanistic explanation: MTF2 is required to maintain silencing at a subset of PRC2 targets, whereas JARID2 is important for the establishment of new repressive *Polycomb* domains that accompany changes in cell identity.

MTF2 and maintenance

Our observation that genes uniquely sensitive to MTF2 depletion display high CpG densities as well as high levels of H3K27me3 in both ESCs and NPCs (Fig. 5; Fig. S5) suggests that MTF2 is required to maintain H3K27me3 at a group of “strong” PRC2 targets that remain repressed during the ESC–NPC transition (Fig. 6B). The high CpG density at these gene promoters may require the MTF2 winged-helix domain (Perino et al., 2018)—which binds

to CG-rich DNA—to recruit PRC2 for maintenance of repression. However, some PRC2 targets with comparable CpG density did not display sensitivity to MTF2 depletion, suggesting that there may be other factors contributing to this requirement.

Given that H3K27me3 can be epigenetically inherited via the read-write function of PRC2 (Hansen et al., 2008; Margueron et al., 2009; Reinberg and Vales, 2018), why would a subset of genes with high H3K27me3 specifically need MTF2 to remain repressed? In *Drosophila,* PRC2 is recruited to its gene targets by *cis*-regulatory sequences called *Polycomb* response elements (PREs) (Schuettengruber et al., 2017). At some targets, the continuous presence of PREs is required for efficient maintenance of H3K27me3 across cell divisions (Coleman and Struhl, 2017; Laprell et al., 2017), suggesting that the read-write H3K27me3 mechanism is not sufficient, at least at a subset of loci. While there is no direct equivalent of PREs in mammals, mammalian PRC2 preferentially localizes at unmethylated CpG islands (CGIs) (Ku et al., 2008; Tanay et al., 2007), and the genomic insertion of exogenous CG-rich DNA results in PRC2 recruitment (Mendenhall et al., 2010). We propose that at a subset of CGIs, similar to PREs in *Drosophila,* the presence of H3K27me3 alone is not sufficient for its maintenance and MTF2 is required for its faithful inheritance—perhaps more so in the context of the vast epigenetic reprogramming that accompanies differentiation. This is in agreement with previous findings in ESCs, where KO of *Mtf2* caused a preferential reduction in H3K27me3 at regions with high densities of GCG motifs (Perino et al., 2018).

JARID2 and establishment

In contrast to MTF2, JARID2 seems to be preferentially required to direct H3K27me3 deposition at genes that are expressed and marked by H3K4me3 in ESCs but silenced in NPCs (Fig. 5), suggesting a specific involvement in the establishment of *Polycomb* domains during cell fate transitions (Fig. 6C). Consistent with this notion, a domain on JARID2 is methylated by the PRC2 catalytic subunit EZH2, resulting in a feedback loop that promotes H3K27me3 deposition (Sanulli et al., 2015). The stimulation of PRC2 by methylation of JARID2 utilizes the same allosteric mechanism employed by H3K27me3 (Justin et al., 2016; Lee et al., 2018b; Sanulli et al., 2015) and can bypass RNA-mediated inhibition of PRC2 (Zhang et al., 2019). Additionally, the presence of JARID2 is sufficient to partially overcome the inhibitory effects of active chromatin marks such as H3K4me3 and H3K36me3 *in vitro* (Kasinath et al., 2021). Thus, we propose that JARID2 is required for the nucleation of new H3K27me3 domains at a subset of loci that lack pre-existing H3K27me3 (Fig. 6C), possibly via PRC2-catalyzed methylation of JARID2.

This raises the question of how JARID2 is recruited to these *de novo* H3K27me3 nucleation sites. Several potential pathways for JARID2 recruitment to chromatin have been proposed, including direct DNA recognition (Kim et al., 2003; Li et al., 2010; Peng et al., 2009; Son et al., 2013), and, more recently, a PRC1–PRC2 crosstalk pathway by which H2AK119ub1 deposited by variant PRC1 is recognized by the JARID2 UIM domain (Blackledge et al., 2020; Cooper et al., 2016; Healy et al., 2019; Tamburri et al., 2020). The structure of JARID2-containing PRC2 in complex with H2AK119bu1 revealed extensive interactions between the UIM domain and the ubiquitin moiety, which might contribute to stimulating PRC2 activity on H2AK119ub1-modified nucleosomes *in vitro* (Kasinath et al., 2021).

These observations can be placed in a functional context by our findings: a subset of genes are “pre-marked” with H2AK119ub1 in ESCs although they are transcribed and carry the active H3K4me3 mark. These genes require the presence of JARID2 for their repression by PRC2 during differentiation because JARID2-containing PRC2.2 is better suited to deposit H3K27me3 on active chromatin. However, not all H3K4me3-marked genes active in ESCs require JARID2 for repression during differentiation, indicating that PRC2 can adopt multiple strategies to establish new H3K27me3 domains.

Concluding remarks

We have discovered that MTF2 (PRC2.1) and JARID2 (PRC2.2) are required for the repression of different sets of genes with distinct chromatin properties and expression dynamics during differentiation. Our findings suggest that PRC2.1 and PRC2.2 contribute to different modalities of *Polycomb* repression, maintenance *vs.* establishment, explaining the distinct effects of their individual KOs during development as well as their redundancy in pluripotent ESCs. Our results also demonstrate the utility of the AID system in dissecting complex regulatory pathways. The ability to rapidly degrade and restore different subunits of PRC2 before, during, or after differentiation will facilitate additional mechanistic insights into this essential epigenetic regulator.

Limitations of the study

We only studied the effects of MTF2 and JARID2 depletion in two differentiation paradigm (neural and cardiac) and of these only the ESC to NPC differentiation was analyzed in great detail. It is possible that MTF2 and JARID2 play different roles in different cellular context and a more comprehensive characterization in multiple systems and, ultimately, during development *in vivo* will be needed to generalize our conclusions. Moreover, additional accessory subunits of PRC2 exist and their roles in the context of maintenance *vs.* establishment was not analyzed in our study. This is particularly important for the two paralogs of MTF2 (PHF1 and PHF19), which might provide some redundancy in function and reduce the impact of MTF2 acute depletion. Finally, although the presence of a distinct set of histone marks (H2AK119ub1 and H3K4me3 in absence of H3K27me3) in ESCs correlates with sensitivity to JARID2 depletion during differentiation, the instructive role of this chromatin structure remains to be formally demonstrated.

STAR METHODS

Resource availability

Lead contact—Further information and requests for resources and reagents should be directed to and will be fulfilled by the Lead Contact, Roberto Bonasio (roberto@bonasiolab.org).

Materials availability—AID-tagged ESC lines are available from the Lead Contact upon request.

Data and code availability—Next generation sequencing data generated for this study have been deposited in the NCBI GEO with accession number GSE155997.

Experimental model and subject details

Mouse embryonic stem cell culture—C57BL/6 mouse ESCs (ATCC SCRC-1002) were cultured on gelatinized dishes in serum-free N2B27 media (1:1 mix of neurobasal medium (Gibco) and DMEM/F12 (Gibco), 100 mM MEM nonessential amino acids (Sigma), 55 μM 2-mercaptoethanol (Gibco), 2 mM L-glutamine (Sigma), 0.5% penicillin/streptomycin (Sigma), 1x N27 (Gibco 17502048) and 1x B27 (Gibco 17504044)) supplemented with 100 U/mL leukemia inhibitory factor (LIF) (Sigma), 3 μM CHIR99021 (Millipore) and 1 μM PD0325901 (Millipore). Cells were passaged every 2–3 days via dissociation in 0.05% trypsin (Genesee Scientific).

Method details

Cell line generation—osTIR1-expressing parental mESCs were generated by CRISPR/Cas9 targeting wild-type C57BL/6 mESCs. Cells were transiently transfected with the pEN396 vector (Addgene #92142) (Nora et al., 2017) modified to contain a zeocin-resistance gene, and the PX459 vector (Addgene #62988) expressing spCas9 and an sgRNA targeting the safe-harbor *TIGRE* locus, followed by selection with 1 μg/mL Puromycin (Invitrogen) for 48 h then selection with 50 μg/Ml Zeocin (Invitrogen) for an additional 4 days. Individual clones were screened by PCR. The genotype of the positive clones was confirmed by Sanger sequencing and western blotting.

AID-tagged mESC lines were generated from the osTIRI-expressing parental line using CRISPR-Cas9 targeting. For each CRISPR targeting, cells were transiently transfected with a donor vector containing an HA epitope and AID (AID*, 44 amino-acids) (Morawska and Ulrich, 2013) fusion tag flanked by 1 -kb homology arms specific to the *Mtf2, Jarid2,* or *Suz12* genomic loci along with the PX459 vector (Addgene #62988) expressing a locus-specific sgRNA and Cas9-T2A-PuroR.. Transfected cells were selected with 1 μg/mL Puromycin (Invitrogen) for 48 h, then cultured for an additional 4 days without antibiotic. Individual clones were picked and screened as described above.

Plasmids and sequences—sgRNA and fusion tag sequences used in this study are listed in the STAR key resources table. For donor plasmid construction, locus-specific 1 -kb homology arms were PCR amplified from wild-type C57BL/6 genomic DNA. The HA–AID fusion tag contains the AID* sequence (Morawska and Ulrich, 2013), and was ordered as a geneBlock from IDT. The locus-specific homology arms and HA-AID fusion tag were inserted into the pINTA-N3 (Kaneko et al., 2013) plasmid backbone using Gibson assembly.

Differentiation to neural progenitors—Differentiation was performed essentially as described in (Gouti et al., 2014). ESCs were seeded in serum-free conditions at a density of 15,000 cells/mL in 6-well plates and incubated for 12 h to allow for cell attachment. For NPC induction, the ESC media was removed and replaced with N2B27 media supplemented with 40 μg/mL BSA (Sigma) and 10 ng/mL bFGF (R&D 3139), and incubated for 72 h with daily media exchanges. Media was then replaced with N2B27 media supplemented with 40 μg/mL BSA (Sigma) and 500 nM SAG (Millipore 566661) for an additional 48 h before harvesting for RNA, chromatin, or western blot analysis.

Differentiation to cardiac precursors—Differentiation was performed essentially as described in (Oh and Ishikawa, 2018; Wamstad et al., 2012). ESCs were seeded on bacterial petri dishes at 75,000 cells/mL and aggregated into embryoid bodies (EBs) for 48h in serum-free differentiation media (3:1 IMDM (Cellgro 15–016-CV) to Ham's F-12 (Cellgro 10–080-CV), 0.05% BSA (Sigma), 2mM L-glutamine (Sigma), 1x N2 (Gibco 17502048), 1x B27 (minus vitamin A, Gibco 12587010)) supplemented with 50 μg/mL L-ascorbic acid (Sigma) and 4.5×10^{-4} M MTG (Sigma M6145). EBs were then dissociated and seeded at 75,000 cells/mL in bacterial petri dishes to reaggregate for 43 hr in the presence of 5 ng/mL human VEGF (R&D 293-VE), human Activin A (R&D 338-AC) and human BMP4 (R&D #314-BP) at concentrations determined empirically (see Note). EBs were dissociated and plated at 300,000 cells/cm^2 for monolayer culture in StemPro-34 (Gibco 10639011) supplemented with 5 ng/mL human VEGF (R&D 293-VE), 10 ng/mL human basic FGF (R&D 233-FB) and 25 ng/mL FGF10 (R&D 345-FG). Cells reached the cardiac precursor stage 32 h after plating in StemPro-34 (Wamstad et al., 2012) and were harvested for RNA analysis.

Note: The differentiation efficiency is very sensitive to the concentrations of BMP4 and Activin A in the media. BMP4 and Activin A concentrations were determined empirically during a trial 8-day differentiation to mature cardiomyocytes (a 3-day extension of the cardiac precursor protocol above). Optimal BMP4 and Activin A concentrations were selected based on the number of beating clusters of cardiomyocytes on day 8. In our hands, we had the most success with 8 ng/mL Activin A and 0.8 ng/mL BMP4.

Auxin treatment—For auxin-inducible degradation of subunits, indole-3-acetic acid (IAA, auxin analog) (Sigma I5148–2G) was added in the culture media at a final concentration of 50 μM (diluted from a 500 mM stock dissolved in sterile water) for the indicated time periods.

Western blotting—Cell lysates were prepared by resuspension in CHAPS/urea lysis buffer (50 mM Tris pH 8_{RT}, 8 M Urea, 1% CHAPS) with cOmplete EDTA-free protease inhibitor (Roche) and quantified with the Bio-Rad Protein Assay Dye Reagent (Bio-Rad). Equal amounts of lysate were denatured in 1X NuPAGE LDS sample buffer (Thermo Fisher) with 10% 2-mercaptoethanol (Sigma) for 10 min at 70 °C followed by SDS-PAGE. Proteins were transferred to nitrocellulose membranes using a Bio-Rad Trans-Blot Turbo. Western-blotting was carried out using the indicated primary antibodies (STAR key resources table) and HRP-conjugated light-chain specific secondary antibodies (Jackson Immunoresearch), and images were acquired with a GE Healthcare Amersham Imager 600.

Co-immunoprecipitation—Cell lysates were prepared in non-denaturing conditions using a 1% NP-40 lysis buffer (50 mM Tris pH 8_{RT}, 150 mM NaCl, 1% NP-40, 0.2 mM EDTA, 2 mM $MgCl_2$) followed by sonication (5 cycles of 30 s ON/30s OFF for a total of 5 min) in a Bioruptor (Diagenode). NaCI was added to the lysates to a final concentration of 300 mM and lysates were incubated at 4 °C with rotation for 30 min. Lysates were then spun at 18,000 g for 5 min at 4 °C, and the supernatant was quantified with the Bio-Rad Protein Assay Dye Reagent (Bio-Rad). Lysates were diluted to a final protein concentration of 1 g/L with IP wash buffer (20 mM Tris pH $7.9_{4\ °C}$, 0.2 mM EDTA, 200 mM KCl, and 0.05%

NP-40) and incubated overnight at 4 °C with either anti-EZH2 (affinity purified) (Zhang et al., 2019) or Rabbit IgG (Jackson Immunoresearch). Dynabeads Protein G were blocked overnight at 4 °C in IP wash buffer with 1 mg/mL BSA (NEB). The next day, the IP samples were spun at 10,000 g for 10 min at 4 °C, and the supernatant was transferred to fresh low-retention tubes. The blocked beads were washed in IP wash buffer, aliquoted into the IP samples, and samples were incubated at 4 °C with rotation for 1 h. Samples were washed and proteins were eluted from beads by adding 1X NuPAGE LDS sample buffer (Thermo Fisher) and boiling at 95 °C for 5 min. SDS-PAGE and western blotting were performed as described above.

RNA isolation, RT-qPCR, and sequencing—Cultured cells were rinsed once with PBS and lysed via direct addition of TRIzol reagent (Thermo Fisher Scientific). Total cellular RNA was purified using the Direct-zol RNA Miniprep kit (Zymo Research) or via PCIA. For RT-qPCR, 25 ng of RNA were assayed per 10 μL reaction using the RNA-to-Ct single-step kit (Thermo Fisher) and *Gapdh* as a normalization control. RT-qPCR primers are listed in the STAR key resources table. For library preparation, polyA+ RNA was isolated from 1.5 μg (ESC and NPC experiments) or 400 ng (CP experiments) total RNA using Dynabeads Oligo (dT)25 beads (Thermo Fisher) and constructed into strand-specific libraries using the dUTP method. UTP-marked cDNA was end-repaired using end-repair mix (Enzymatics), tailed with deoxyadenine using Klenow exo- (Enzymatics), and ligated to custom dual indexed adapters with T4 DNA ligase (Enzymatics). Libraries were size-selected with SPRIselect beads (Beckman Coulter) and quantified by qPCR after amplification. Paired-end sequencing was performed on a NextSeq 500 (Illumina).

CUT&RUN—CUT&RUN was performed as described online by Meers and Henikoff at https://www.protocols.io/view/cut-amp-run-targeted-in-situ-genome-wide-profiling-zcpf2vn. Briefly, cell cultures were harvested, washed and counted with the Countess Automated Cell Counter (Invitrogen). Equal numbers of cells per condition were bound to Concanavalin A-coated magnetic beads (Bangs laboratories), and then permeabilized with 0.015% dig-wash buffer (20 mM HEPES pH 7.5, 150 mM, NaCI, 0.5 mM spermidine, one Roche complete EDTA-free tablet per 50 ml, and 0.015% digitonin). Following bead binding, the supernatant was discarded and the bead-cell slurry was resuspended in 150 μl antibody buffer (0.015% dig-wash buffer with 2 mM EDTA) containing primary antibody. Antibody incubation was carried out for 2 h or overnight at 4 °C on a nutator. Samples were washed with dig-wash buffer to remove unbound antibody, then incubated with Protein A-MNase (700 ng/mL, kind gift of the Sarma lab) in dig-wash buffer for 1 h at 4 °C on a nutator. Samples were then washed with dig-wash buffer, resuspended in 100 μL dig-wash buffer and cooled to 0 °C on a metal tube rack on ice for 5 min. 2 μL 100 mM $CaCl_2$ was added per sample to activate the MNase, and samples were digested for 30 min at 0 °C. The digestion reactions were quenched via addition of 100 μl 2X STOP Buffer (340 mM NaCl, 20 mM EDTA, 4 mM EGTA, 0.015% digitonin, 100 μg/mL RNAse A (Thermo Fisher), 50 ug/mL glycoblue (Thermo Fisher), and 100 pg/mL *Drosophila* S2 spike-in DNA (sonicated to ~200bp). Samples were then incubated for 30 min at 37 °C to release CUT&RUN fragments. Supernatant containing CUT&RUN elutions was transferred to fresh tubes and DNA was purified using the MinElute PCR Purification Kit (Qiagen). Purified DNA was quantified

using the Qubit dsDNA HS Assay (Thermo Fisher), then used to make sequencing libraries. Paired-end sequencing was performed on a NextSeq 500 (Illumina).

Quantification and statistical analysis

RNA sequencing analysis—Paired-end RNA-seq reads were aligned the *Mus musculus* mm10 genome using STAR 2.6.1d (Dobin et al., 2013) with default parameters except –*peOverlapNbasesMin* set to 10 and –*alignIntronMax* set to 100000. Differentially expressed genes were identified with DESeq2 (Love et al., 2014) in R using a cutoff of adjusted p-value < 0.1 and fold-change > 1.5. Differential gene expression was visualized by MA plots using the log2 (fold-change) calculated from RPKMs. Heatmaps were generated using the pheatmap package (Kolde, 2019). Individual gene bar plots were generated in GraphPad Prism (GraphPad Software Inc) using TPM (transcripts per million) normalization.

Gene Ontology (GO) analysis—GO terms associated with gene sets were obtained with the topGO package (Alexa and Rahnenfuhrer, 2019) in R using the Biological Process (BP) ontology database. *P*-values for term enrichment were obtained using the “weight01” algorithm with Fisher’s exact test. GO term enrichments were plotted as -log 10 (*P*-value) using ggplot2 (Wickham, 2016).

CUT&RUN analysis—Paired-end CUT&RUN reads were aligned the *M. musculus* mm10 genome using Bowtie2 (Langmead and Salzberg, 2012) version 2.3.4.3 with the *--maxins* parameter set to 2500, and the *--no-unal, --very-sensitive,* and *--no-discordant* options selected. Duplicated reads were marked using MarkDuplicates with Picard v2.19 (Broad Institute, 2019) and were excluded from downstream analyses. Peaks of SUZ12 occupancy were called using MACS2 (Zhang et al., 2008); blacklisted regions and peaks also identified in the IgG condition were subtracted from the SUZ12 peak list to obtain a list of high confidence peaks. PRC2 targets for the NPC differentiation were defined as genes whose TSS was in the vicinity (<50 kb) of SUZ12 peaks identified in either ESCs or NPCs (this study). PRC2 targets for the CP differentiation were defined as genes whose TSS was in the vicinity (<50 kb) of SUZ12 peaks identified in ESCs (this study) or H3K27me3 peaks identified in CPs (data from (Wamstad et al., 2012)). Heatmaps for SUZ12, JARID2, and MTF2 occupancy centered on SUZ12 peaks were generated by summing CPM-normalized counts from 10 bp bins spanning ± 3 kb from each peak center, and visualized with the pheatmap package in R. For heatmap comparisons of global changes in occupancy of H3K27me3, H3K4me3, MTF2, or JARID2 before and after auxin treatment, raw counts spanning ± 10 kb (H3K27me3) or ± 3kb (H3K4me3, MTF2, JARID2) from each peak center were normalized to the total number of reads mapping to the *D. melanogaster* dm6 genome (spike-in reads). Violin plots for H3K27me3, SUZ12, H3K4me3, and H2AK119ub1 density at the TSS were generated by summing the CPM-normalized counts in a ± 2.5 kb window surrounding the validated NCBI RefSeqTSS of the indicated gene sets, and visualized using ggplot2.

Bivalent genes analysis—Bivalent genes in NPCs were defined using H3K27me3 and H3K4me3 CUT&RUN data generated from WT NPCs in this study. Bivalent genes were

defined as genes whose TSS region (+/− 2.5 kb from RefSeqTSS) exhibited at least a 3-fold enrichment of both H3K27me3 and H3K4me3 spike-in normalized counts over IgG signal.

Calculation of CpG densities—Promoter CpG densities were calculated in a −1000bp/+100bp region surrounding the TSS of the indicated gene sets using the cpgDensityCalc function from the Repitools package (Statham et al., 2010). CpG density was defined as the number of CpG dinucleotides detected in the specified window.

Statistics—Sample size and statistical tests are indicated in the figure legends. Unless otherwise noted all statistical tests were two-sided. All replicates were obtained by measuring distinct samples (biological and/or experimental replicates) and not by measuring multiple times the same sample (technical replicates). Boxplots were drawn using default parameters in R (center line, median; box limits, upper and lower quartiles; whiskers, 1.5x interquartile range). In all violin plots, the boxes indicate median and interquartile range.

Supplementary Material

Refer to Web version on PubMed Central for supplementary material.

ACKNOWLEDGMENTS

The authors thank K. Sarma, E. Shields, R. Warneford-Thomson, and D. Reinberg for critical reading of the manuscript. We also thank the Sarma lab for the kind gift of purified pA-MNase. A. P. was supported in part by a training grant and an NRSA predoctoral fellowship from the NIH (T32 HD083185 and F31HD102121). This work was supported in part by NIH grants R01GM127408 and R01GM138788 to R.B.

REFERENCES

Alexa A, and Rahnenfuhrer J (2019). topGO: Enrichment Analysis for Gene Ontology.

Ballare C, Lange M, Lapinaite A, Martin GM, Morey L, Pascual G, Liefke R, Simon B, Shi Y, Gozani O, et al. (2012). Phf19 links methylated Lys36 of histone H3 to regulation of Polycomb activity. Nat Struct Mol Biol 19, 1257–1265. [PubMed: 23104054]

Beringer M, Pisano P, Di Carlo V, Blanco E, Chammas P, Vizan P, Gutierrez A, Aranda S, Payer B, Wierer M, et al. (2016). EPOP Functionally Links Elongin and Polycomb in Pluripotent Stem Cells. Mol Cell 64, 645–658. [PubMed: 27863225]

Bertrand N, Castro DS, and Guillemot F (2002). Proneural genes and the specification of neural cell types. Nat Rev Neurosci 3, 517–530. [PubMed: 12094208]

Blackledge NP, Fursova NA, Kelley JR, Huseyin MK, Feldmann A, and Klose RJ (2020). PRC1 Catalytic Activity Is Central to Polycomb System Function. Mol Cell 77, 857–874 e859. [PubMed: 31883950]

Boyer LA, Plath K, Zeitlinger J, Brambrink T, Medeiros LA, Lee TI, Levine SS, Wernig M, Tajonar A, Ray MK, et al. (2006). Polycomb complexes repress developmental regulators in murine embryonic stem cells. Nature 441, 349–353. [PubMed: 16625203]

Bracken AP, and Helin K (2009). Polycomb group proteins: navigators of lineage pathways led astray in cancer. Nat Rev Cancer 9, 773–784. [PubMed: 19851313]

Brien GL, Gambero G, O'Connell DJ, Jerman E, Turner SA, Egan CM, Dunne EJ, Jurgens MC, Wynne K, Piao L, et al. (2012). Polycomb PHF19 binds H3K36me3 and recruits PRC2 and demethylase NO66 to embryonic stem cell genes during differentiation. Nat Struct Mol Biol 19, 1273–1281. [PubMed: 23160351]

Chen S, Jiao L, Liu X, Yang X, and Liu X (2020). A Dimeric Structural Scaffold for PRC2-PCL Targeting to CpG Island Chromatin. Mol Cell 77, 1265–1278 e1267. [PubMed: 31959557]

Chen S, Jiao L, Shubbar M, Yang X, and Liu X (2018). Unique Structural Platforms of Suz12 Dictate Distinct Classes of PRC2 for Chromatin Binding. Mol Cell 69, 840–852 e845. [PubMed: 29499137]

Choi J, Bachmann AL, Tauscher K, Benda C, Fierz B, and Muller J (2017). DNA binding by PHF1 prolongs PRC2 residence time on chromatin and thereby promotes H3K27 methylation. Nat Struct Mol Biol 24, 1039–1047. [PubMed: 29058710]

Coleman RT, and Struhl G (2017). Causal role for inheritance of H3K27me3 in maintaining the OFF state of a Drosophila HOX gene. Science 356.

Comet I, Riising EM, Leblanc B, and Helin K (2016). Maintaining cell identity: PRC2-mediated regulation of transcription and cancer. Nat Rev Cancer 16, 803–810. [PubMed: 27658528]

Conway E, Jerman E, Healy E, Ito S, Holoch D, Oliviero G, Deevy O, Glancy E, Fitzpatrick DJ, Mucha M, et al. (2018). A Family of Vertebrate-Specific Polycombs Encoded by the LCOR/LCORL Genes Balance PRC2 Subtype Activities. Mol Cell 70, 408–421 e408. [PubMed: 29628311]

Cooney E, Bi W, Schlesinger AE, Vinson S, and Potocki L (2017). Novel EED mutation in patient with Weaver syndrome. Am J Med Genet A 173, 541–545. [PubMed: 27868325]

Cooper S, Grijzenhout A, Underwood E, Ancelin K, Zhang T, Nesterova TB, Anil-Kirmizitas B, Bassett A, Kooistra SM, Agger K, et al. (2016). Jarid2 binds mono-ubiquitylated H2A lysine 119 to mediate crosstalk between Polycomb complexes PRC1 and PrC2. Nat Commun 7, 13661. [PubMed: 27892467]

Cruz-Molina S, Respuela P, Tebartz C, Kolovos P, Nikolic M, Fueyo R, van Ijcken WFJ, Grosveld F, Frommolt P, Bazzi H, et al. (2017). PRC2 Facilitates the Regulatory Topology Required for Poised Enhancer Function during Pluripotent Stem Cell Differentiation. Cell Stem Cell 20, 689–705 e689. [PubMed: 28285903]

Dobin A, Davis CA, Schlesinger F, Drenkow J, Zaleski C, Jha S, Batut P, Chaisson M, and Gingeras TR (2013). STAR: ultrafast universal RNA-seq aligner. Bioinformatics 29, 15–21. [PubMed: 23104886]

Duncan IM (1982). Polycomblike: a gene that appears to be required for the normal expression of the bithorax and antennapedia gene complexes of Drosophila melanogaster. Genetics 102, 49–70. [PubMed: 6813190]

Faust C, Schumacher A, Holdener B, and Magnuson T (1995). The eed mutation disrupts anterior mesoderm production in mice. Development 121, 273–285. [PubMed: 7768172]

Gibson WT, Hood RL, Zhan SH, Bulman DE, Fejes AP, Moore R, Mungall AJ, Eydoux P, Babul-Hirji R, An J, et al. (2012). Mutations in EZH2 cause Weaver syndrome. Am J Hum Genet 90, 110–118. [PubMed: 22177091]

Gouti M, Tsakiridis A, Wymeersch FJ, Huang Y, Kleinjung J, Wilson V, and Briscoe J (2014). In vitro generation of neuromesodermal progenitors reveals distinct roles for wnt signalling in the specification of spinal cord and paraxial mesoderm identity. PLoS Biol 12, e1001937. [PubMed: 25157815]

Grosswendt S, Kretzmer H, Smith ZD, Kumar AS, Hetzel S, Wittier L, Klages S, Timmermann B, Mukherji S, and Meissner A (2020). Epigenetic regulator function through mouse gastrulation. Nature 584, 102–108. [PubMed: 32728215]

Hansen KH, Bracken AP, Pasini D, Dietrich N, Gehani SS, Monrad A, Rappsilber J, Lerdrup M, and Helin K (2008). A model for transmission of the H3K27me3 epigenetic mark. Nat Cell Biol 10, 1291–1300. [PubMed: 18931660]

Hauri S, Comoglio F, Seimiya M, Gerstung M, Glatter T, Hansen K, Aebersold R, Paro R, Gstaiger M, and Beisel C (2016). A High-Density Map for Navigating the Human Polycomb Complexome. Cell Rep 17, 583–595. [PubMed: 27705803]

Healy E, Mucha M, Glancy E, Fitzpatrick DJ, Conway E, Neikes HK, Monger C, Van Mierlo G, Baltissen MP, Koseki Y, et al. (2019). PRC2.1 and PRC2.2 Synergize to Coordinate H3K27 Trimethylation. Mol Cell 76, 437–452 e436. [PubMed: 31521505]

Herz HM, Mohan M, Garrett AS, Miller C, Casto D, Zhang Y, Seidel C, Haug JS, Florens L, Washburn MP, et al. (2012). Polycomb repressive complex 2-dependent and - independent

functions of Jarid2 in transcriptional regulation in Drosophila. Mol Cell Biol 32, 1683–1693. [PubMed: 22354997]

Hojfeldt JW, Hedehus L, Laugesen A, Tatar T, Wiehle L, and Helin K (2019). Non-core Subunits of the PRC2 Complex Are Collectively Required for Its Target-Site Specificity. Mol Cell 76, 423–436 e423. [PubMed: 31521506]

Hojfeldt JW, Laugesen A, Willumsen BM, Damhofer H, Hedehus L, Tvardovskiy A, Mohammad F, Jensen ON, and Helin K (2018). Accurate H3K27 methylation can be established de novo by SUZ12-directed PRC2. Nat Struct Mol Biol 25, 225–232. [PubMed: 29483650]

Howe FS, Fischl H, Murray SC, and Mellor J (2017). Is H3K4me3 instructive for transcription activation? Bioessays 39, 1–12.

Imagawa E, Albuquerque EVA, Isidor B, Mitsuhashi S, Mizuguchi T, Miyatake S, Takata A, Miyake N, Boguszewski MCS, Boguszewski CL, et al. (2018). Novel SUZ12 mutations in Weaver-like syndrome. Clin Genet 94, 461–466. [PubMed: 30019515]

Jadhav U, Nalapareddy K, Saxena M, O'Neill NK, Pinello L, Yuan GC, Orkin SH, and Shivdasani RA (2016). Acquired Tissue-Specific Promoter Bivalency Is a Basis for PRC2 Necessity in Adult Cells. Cell 165, 1389–1400. [PubMed: 27212235]

Justin N, Zhang Y, Tarricone C, Martin SR, Chen S, Underwood E, De Marco V, Haire LF, Walker PA, Reinberg D, et al. (2016). Structural basis of oncogenic histone H3K27M inhibition of human polycomb repressive complex 2. Nat Commun 7, 11316. [PubMed: 27121947]

Kalb R, Latwiel S, Baymaz HI, Jansen PW, Muller CW, Vermeulen M, and Muller J (2014). Histone H2A monoubiquitination promotes histone H3 methylation in Polycomb repression. Nat Struct Mol Biol 21, 569–571. [PubMed: 24837194]

Kaneko S, Son J, Shen SS, Reinberg D, and Bonasio R (2013). PRC2 binds active promoters and contacts nascent RNAs in embryonic stem cells. Nat Struct Mol Biol 20, 1258–1264. [PubMed: 24141703]

Kasinath V, Beck C, Sauer P, Poepsel S, Kosmatka J, Faini M, Toso D, Aebersold R, and Nogales E (2021). JARID2 and AEBP2 regulate PRC2 in the presence of H2AK119ub1 and other histone modifications. Science 371.

Kim TG, Kraus JC, Chen J, and Lee Y (2003). JUMONJI, a critical factor for cardiac development, functions as a transcriptional repressor. J Biol Chem 278, 42247–42255. [PubMed: 12890668]

Kloet SL, Makowski MM, Baymaz HI, van Voorthuijsen L, Karemaker ID, Santanach A, Jansen P, Di Croce L, and Vermeulen M (2016). The dynamic interactome and genomic targets of Polycomb complexes during stem-cell differentiation. Nat Struct Mol Biol 23, 682–690. [PubMed: 27294783]

Kolde R (2019). pheatmap: Pretty Heatmaps.

Ku M, Koche RP, Rheinbay E, Mendenhall EM, Endoh M, Mikkelsen TS, Presser A, Nusbaum C, Xie X, Chi AS, et al. (2008). Genomewide analysis of PRC1 and pRc2 occupancy identifies two classes of bivalent domains. PLoS Genet 4, e1000242. [PubMed: 18974828]

Langmead B, and Salzberg SL (2012). Fast gapped-read alignment with Bowtie 2. Nat Methods 9, 357–359. [PubMed: 22388286]

Laprell F, Finkl K, and Muller J (2017). Propagation of Polycomb-repressed chromatin requires sequence-specific recruitment to DNA. Science 356, 85–88. [PubMed: 28302792]

Laugesen A, Hojfeldt JW, and Helin K (2019). Molecular Mechanisms Directing PRC2 Recruitment and H3K27 Methylation. Mol Cell 74, 8–18. [PubMed: 30951652]

Lee CH, Holder M, Grau D, Saldana-Meyer R, Yu JR, Ganai RA, Zhang J, Wang M, LeRoy G, Dobenecker MW, et al. (2018a). Distinct Stimulatory Mechanisms Regulate the Catalytic Activity of Polycomb Repressive Complex 2. Mol Cell 70, 435–448 e435. [PubMed: 29681498]

Lee CH, Yu JR, Kumar S, Jin Y, LeRoy G, Bhanu N, Kaneko S, Garcia BA, Hamilton AD, and Reinberg D (2018b). Allosteric Activation Dictates PRC2 Activity Independent of Its Recruitment to Chromatin. Mol Cell 70, 422–434 e426. [PubMed: 29681499]

Lendahl U, Zimmerman LB, and McKay RD (1990). CNS stem cells express a new class of intermediate filament protein. Cell 60, 585–595. [PubMed: 1689217]

Li G, Margueron R, Ku M, Chambon P, Bernstein BE, and Reinberg D (2010). Jarid2 and PRC2, partners in regulating gene expression. Genes Dev 24, 368–380. [PubMed: 20123894]

Li H, Liefke R, Jiang J, Kurland JV, Tian W, Deng P, Zhang W, He Q, Patel DJ, Bulyk ML, et al. (2017). Polycomb-like proteins link the PRC2 complex to CpG islands. Nature 549, 287–291. [PubMed: 28869966]

Liefke R, Karwacki-Neisius V, and Shi Y (2016). EPOP Interacts with Elongin BC and USP7 to Modulate the Chromatin Landscape. Mol Cell 64, 659–672. [PubMed: 27863226]

Love MI, Huber W, and Anders S (2014). Moderated estimation of fold change and dispersion for RNA-seq data with DESeq2. Genome Biol 15, 550. [PubMed: 25516281]

Margueron R, Justin N, Ohno K, Sharpe ML, Son J, Drury WJ 3rd, Voigt P, Martin SR, Taylor WR, De Marco V, et al. (2009). Role of the polycomb protein EED in the propagation of repressive histone marks. Nature 461, 762–767. [PubMed: 19767730]

Margueron R, Li G, Sarma K, Blais A, Zavadil J, Woodcock CL, Dynlacht BD, and Reinberg D (2008). Ezh1 and Ezh2 maintain repressive chromatin through different mechanisms. Mol Cell 32, 503–518. [PubMed: 19026781]

Martinez-Cerdeno V, and Noctor SC (2018). Neural Progenitor Cell Terminology. Front Neuroanat 12, 104. [PubMed: 30574073]

Mendenhall EM, Koche RP, Truong T, Zhou VW, Issac B, Chi AS, Ku M, and Bernstein BE (2010). GC-rich sequence elements recruit PRC2 in mammalian ES cells. PLoS Genet 6, e1001244. [PubMed: 21170310]

Morawska M, and Ulrich HD (2013). An expanded tool kit for the auxin-inducible degron system in budding yeast. Yeast 30, 341–351. [PubMed: 23836714]

Motoyama J, Kitajima K, Kojima M, Kondo S, and Takeuchi T (1997). Organogenesis of the liver, thymus and spleen is affected in jumonji mutant mice. Mech Dev 66, 27–37. [PubMed: 9376320]

Nekrasov M, Klymenko T, Fraterman S, Papp B, Oktaba K, Kocher T, Cohen A, Stunnenberg HG, Wilm M, and Muller J (2007). Pcl-PRC2 is needed to generate high levels of H3-K27 trimethylation at Polycomb target genes. EMBO J 26, 4078–4088. [PubMed: 17762866]

Nishimura K, Fukagawa T, Takisawa H, Kakimoto T, and Kanemaki M (2009). An auxin-based degron system for the rapid depletion of proteins in nonplant cells. Nat Methods 6, 917–922. [PubMed: 19915560]

Nora EP, Goloborodko A, Valton AL, Gibcus JH, Uebersohn A, Abdennur N, Dekker J, Mirny LA, and Bruneau BG (2017). Targeted Degradation of CTCF Decouples Local Insulation of Chromosome Domains from Genomic Compartmentalization. Cell 169, 930–944 e922. [PubMed: 28525758]

O'Carroll D, Erhardt S, Pagani M, Barton SC, Surani MA, and Jenuwein T (2001). The polycomb-group gene Ezh2 is required for early mouse development. Mol Cell Biol 21, 4330–4336. [PubMed: 11390661]

Oh JG, and Ishikawa K (2018). Experimental Models of Cardiovascular Diseases: Overview. In Experimental Models of Cardiovascular Diseases: Methods and Protocols, Ishikawa K, ed. (New York, NY: Springer New York), pp. 3–14.

Oksuz O, Narendra V, Lee CH, Descostes N, LeRoy G, Raviram R, Blumenberg L, Karch K, Rocha PP, Garcia BA, et al. (2018). Capturing the Onset of PRC2-Mediated Repressive Domain Formation. Mol Cell 70, 1149–1162 e1145. [PubMed: 29932905]

Oliviero G, Brien GL, Waston A, Streubel G, Jerman E, Andrews D, Doyle B, Munawar N, Wynne K, Crean J, et al. (2016). Dynamic Protein Interactions of the Polycomb Repressive Complex 2 during Differentiation of Pluripotent Cells. Mol Cell Proteomics 15, 3450–3460. [PubMed: 27634302]

Pasini D, Bracken AP, Jensen MR, Lazzerini Denchi E, and Helin K (2004). Suz12 is essential for mouse development and for EZH2 histone methyltransferase activity. EMBO J 23, 4061–4071. [PubMed: 15385962]

Peng JC, Valouev A, Swigut T, Zhang J, Zhao Y, Sidow A, and Wysocka J (2009). Jarid2/Jumonji coordinates control of PRC2 enzymatic activity and target gene occupancy in pluripotent cells. Cell 139, 1290–1302. [PubMed: 20064375]

Perino M, van Mierlo G, Karemaker ID, van Genesen S, Vermeulen M, Marks H, van Heeringen SJ, and Veenstra GJC (2018). MTF2 recruits Polycomb Repressive Complex 2 by helical-shape-selective DNA binding. Nat Genet 50, 1002–1010. [PubMed: 29808031]

Petryszak R, Keays M, Tang YA, Fonseca NA, Barrera E, Burdett T, Fullgrabe A, Fuentes AM, Jupp S, Koskinen S, et al. (2016). Expression Atlas update--an integrated database of gene and protein expression in humans, animals and plants. Nucleic Acids Res 44, D746–752. [PubMed: 26481351]

Reinberg D, and Vales LD (2018). Chromatin domains rich in inheritance. Science 361, 33–34. [PubMed: 29976815]

Rothberg JLM, Maganti HB, Jrade H, Porter CJ, Palidwor GA, Cafariello C, Battaion HL, Khan ST, Perkins TJ, Paulson RF, et al. (2018). Mtf2-PRC2 control of canonical Wnt signaling is required for definitive erythropoiesis. Cell Discov 4, 21. [PubMed: 29736258]

Sanulli S, Justin N, Teissandier A, Ancelin K, Portoso M, Caron M, Michaud A, Lombard B, da Rocha ST, Offer J, et al. (2015). Jarid2 Methylation via the PRC2 Complex Regulates H3K27me3 Deposition during Cell Differentiation. Mol Cell 57, 769–783. [PubMed: 25620564]

Sarma K, Margueron R, Ivanov A, Pirrotta V, and Reinberg D (2008). Ezh2 requires PHF1 to efficiently catalyze H3 lysine 27 trimethylation in vivo. Mol Cell Biol 28, 2718–2731. [PubMed: 18285464]

Schuettengruber B, Bourbon HM, Di Croce L, and Cavalli G (2017). Genome Regulation by Polycomb and Trithorax: 70 Years and Counting. Cell 171, 34–57. [PubMed: 28938122]

Son J, Shen SS, Margueron R, and Reinberg D (2013). Nucleosome-binding activities within JARID2 and EZH1 regulate the function of PRC2 on chromatin. Genes Dev 27, 2663–2677. [PubMed: 24352422]

Statham AL, Strbenac D, Coolen MW, Stirzaker C, Clark SJ, and Robinson MD (2010). Repitools: an R package for the analysis of enrichment-based epigenomic data. Bioinformatics 26, 1662–1663. [PubMed: 20457667]

Takahashi M, Kojima M, Nakajima K, Suzuki-Migishima R, Motegi Y, Yokoyama M, and Takeuchi T (2004). Cardiac abnormalities cause early lethality of jumonji mutant mice. Biochem Biophys Res Commun 324, 1319–1323. [PubMed: 15504358]

Takeuchi T, Kojima M, Nakajima K, and Kondo S (1999). jumonji gene is essential for the neurulation and cardiac development of mouse embryos with a C3H/He background. Mech Dev 86, 29–38. [PubMed: 10446263]

Takeuchi T, Yamazaki Y, Katoh-Fukui Y, Tsuchiya R, Kondo S, Motoyama J, and Higashinakagawa T (1995). Gene trap capture of a novel mouse gene, jumonji, required for neural tube formation. Genes Dev 9, 1211–1222. [PubMed: 7758946]

Tamburri S, Lavarone E, Fernandez-Perez D, Conway E, Zanotti M, Manganaro D, and Pasini D (2020). Histone H2AK119 Mono-Ubiquitination Is Essential for Polycomb-Mediated Transcriptional Repression. Mol Cell 77, 840–856 e845. [PubMed: 31883952]

Tanay A, O'Donnell AH, Damelin M, and Bestor TH (2007). Hyperconserved CpG domains underlie Polycomb-binding sites. Proc Natl Acad Sci U S A 104, 5521–5526. [PubMed: 17376869]

Tatton-Brown K, Hanks S, Ruark E, Zachariou A, Duarte Sdel V, Ramsay E, Snape K, Murray A, Perdeaux ER, Seal S, et al. (2011). Germline mutations in the oncogene EZH2 cause Weaver syndrome and increased human height. Oncotarget 2, 1127–1133. [PubMed: 22190405]

Walker E, Chang WY, Hunkapiller J, Cagney G, Garcha K, Torchia J, Krogan NJ, Reiter JF, and Stanford WL (2010). Polycomb-like 2 associates with PRC2 and regulates transcriptional networks during mouse embryonic stem cell self-renewal and differentiation. Cell Stem Cell 6, 153–166. [PubMed: 20144788]

Wamstad JA, Alexander JM, Truty RM, Shrikumar A, Li F, Eilertson KE, Ding H, Wylie JN, Pico AR, Capra JA, et al. (2012). Dynamic and coordinated epigenetic regulation of developmental transitions in the cardiac lineage. Cell 151, 206–220. [PubMed: 22981692]

Wickham H (2016). ggplot2: Elegant Graphics for Data Analysis (New York: Springer-Verlag).

Wood HB, and Episkopou V (1999). Comparative expression of the mouse Sox1, Sox2 and Sox3 genes from pre-gastrulation to early somite stages. Mech Dev 86, 197–201. [PubMed: 10446282]

Yu JR, Lee CH, Oksuz O, Stafford JM, and Reinberg D (2019). PRC2 is high maintenance. Genes Dev 33, 903–935. [PubMed: 31123062]

Zeng H, Horie K, Madisen L, Pavlova MN, Gragerova G, Rohde AD, Schimpf BA, Liang Y, Ojala E, Kramer F, et al. (2008). An inducible and reversible mouse genetic rescue system. PLoS Genet 4, e1000069. [PubMed: 18464897]

Zhang Q, McKenzie NJ, Warneford-Thomson R, Gail EH, Flanigan SF, Owen BM, Lauman R, Levina V, Garcia BA, Schittenhelm RB, et al. (2019). RNA exploits an exposed regulatory site to inhibit the enzymatic activity of PRC2. Nat Struct Mol Biol 26, 237–247. [PubMed: 30833789]

Zhang Y, Liu T, Meyer CA, Eeckhoute J, Johnson DS, Bernstein BE, Nusbaum C, Myers RM, Brown M, Li W, et al. (2008). Model-based analysis of ChIP-Seq (MACS). Genome Biol 9, R137. [PubMed: 18798982]

Zhang Z, Jones A, Sun CW, Li C, Chang CW, Joo HY, Dai Q, Mysliwiec MR, Wu LC, Guo Y, et al. (2011). PRC2 complexes with JARID2, MTF2, and esPRC2p48 in ES cells to modulate ES cell pluripotency and somatic cell reprogramming. Stem Cells 29, 229–240. [PubMed: 21732481]

Highlights

- Acute depletion of MTF2 or JARID2 in NPC differentiation affects distinct gene sets
- MTF2-specific genes are silent and carry H3K27me3 in both ESCs and NPCs
- JARID2-specific genes are active in ESCs and become *de novo* silenced in NPCs
- JARID2-specific genes are “pre-marked” by H2AK119ub1 in ESCs despite being active

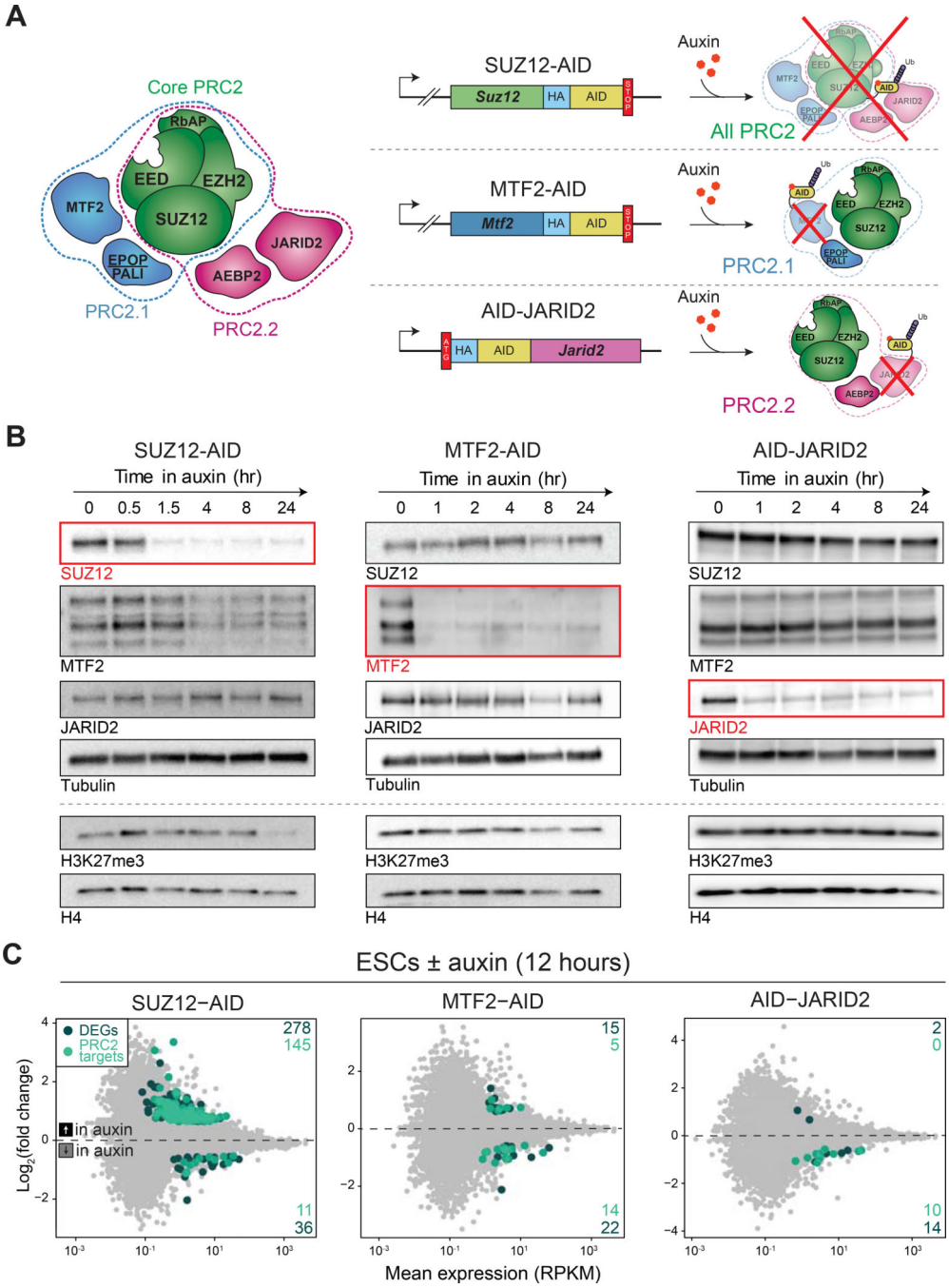

Figure 1. Rapid and specific degradation of PRC2 subunits

(A) Insertion of AID tag at the *Suz12, Mtf2,* or *Jarid2* locus (left), and expected degradation result following auxin treatment (right).

(B) Western blots of whole cell extracts following auxin treatment in the indicated AID-tagged ESC lines.

(C) RNA-seq of the AID-tagged lines in the ESC state comparing 12-hour auxin treatment with control. Differentially expressed genes (FDR <10% and fold-change >1.5) are in dark green and PRC2 target genes are in light green. Data from three biological replicates.

See also Figure S1.

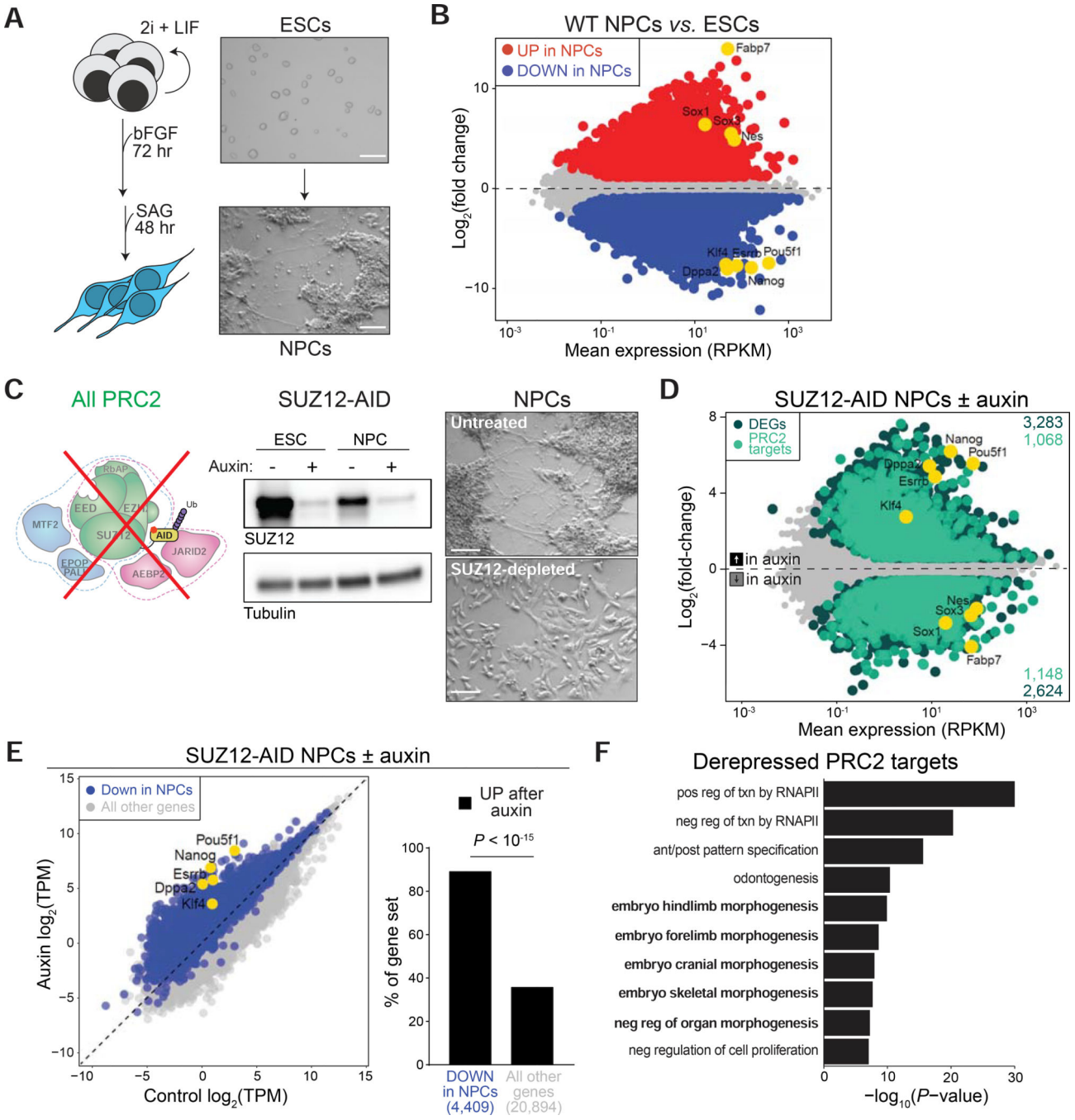

Figure 2. Depletion of core PRC2 impairs NPC differentiation

(A) Protocol for NPC differentiation and brightfield images of cells at the ESC and NPC stage. Scale bars represent 100 μm.

(B) MA plot of RNA-seq in WT ESCs (day 0) and NPCs (day 5 of differentiation). Genes significantly upregulated in NPCs are in red and dowregulated genes are in blue (FDR 10% and $|\log_2\text{-fold-change}| > 1$). Pluripotency- and NPC-associated genes are in yellow. Data from three biological replicates per condition.

(C) Left: western blot of SUZ12 depletion in ESCs (day 0) and NPCs (day 5). Right: brightfield images of untreated and auxin-treated SUZ12-AID cells at day 5. Scale bars represent 100 μm.
(D) MA plot of RNA-seq in SUZ12-AID cells on day 5 of differentiation. Differentially expressed genes are in dark green (FDR < 10% and fold-change > 1.5), and PRC2 target genes are in light green. Data from three biological replicates.
(E) Left: scatter-plot of $\log_2$(transcripts per million (TPM)) from untreated (x-axis) and auxin-treated (y-axis) SUZ12-AID cells on day 5. Genes significantly downregulated during the ESC–NPC transition (B) are in blue. Right: % of genes upregulated after auxin treatment in the indicated classes. *P*-value is from a Fisher's exact test. Data from two (auxin) or three (control) biological replicates.
(F) GO-term enrichment analysis of auxin-upregulated genes that are also PRC2 targets. GO terms related to embryonic development are in bold.
See also Figure S2.

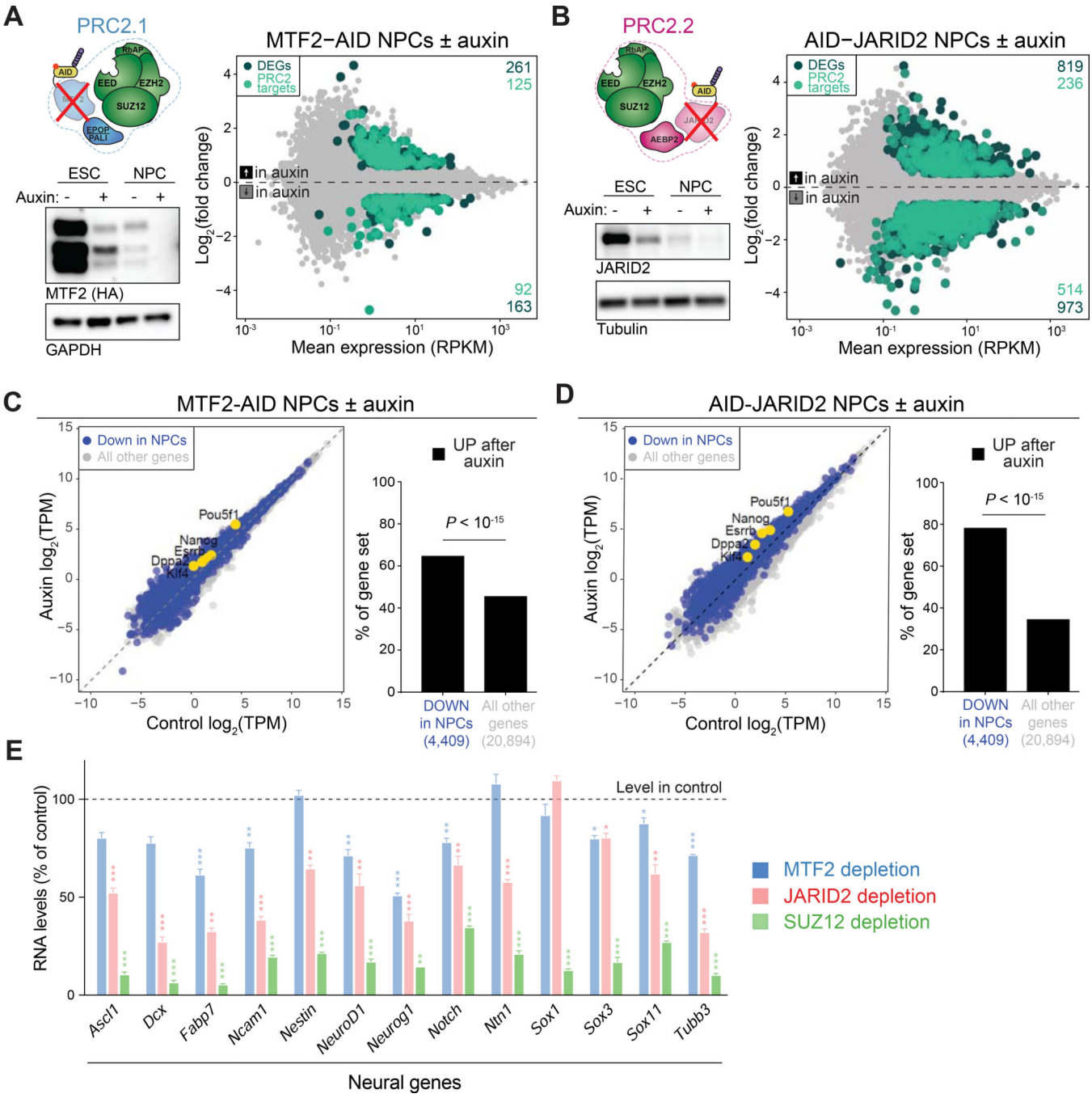

Figure 3. MTF2 and JARID2 are independently required for NPC differentiation

(A) Left: western blot of MTF2 depletion on day 0 (ESC) and day 5 (NPC) of neural differentiation. Right: RNA-seq in MTF2-AID cells at day 5 of differentiation ± auxin. Differential genes are in dark green (FDR < 10% and fold-change > 1.5) and PRC2 target genes are in light green. Data from three biological replicates.

(B) Same as (A) but for AID-JARID2 cells.

(C) Left: Pairwise scatter-plot of $\log_2$(TPM) from untreated (x-axis) and auxin-treated (y-axis) MTF2-AID cells on day 5; genes significantly downregulated at day 5 in WT cells

(from Fig. 2B) are in blue. Right: % of genes upregulated after auxin treatment in the indicated classes. *P*-value is from a Fisher's exact test.

(D) Same as (C) but for AID-JARID2 cells.

(E) RNA levels for neural identity genes in auxin-treated cells relative to untreated cells at day 5 of differentiation, expressed as % of control. Bars represent the mean + SEM. Data from three biological replicates. *, $P < 0.05$; **, $P < 0.01$; ***, $P < 0.001$ from t-tests with Benjamini-Hochberg multiple testing correction.

See also Figure S3A.

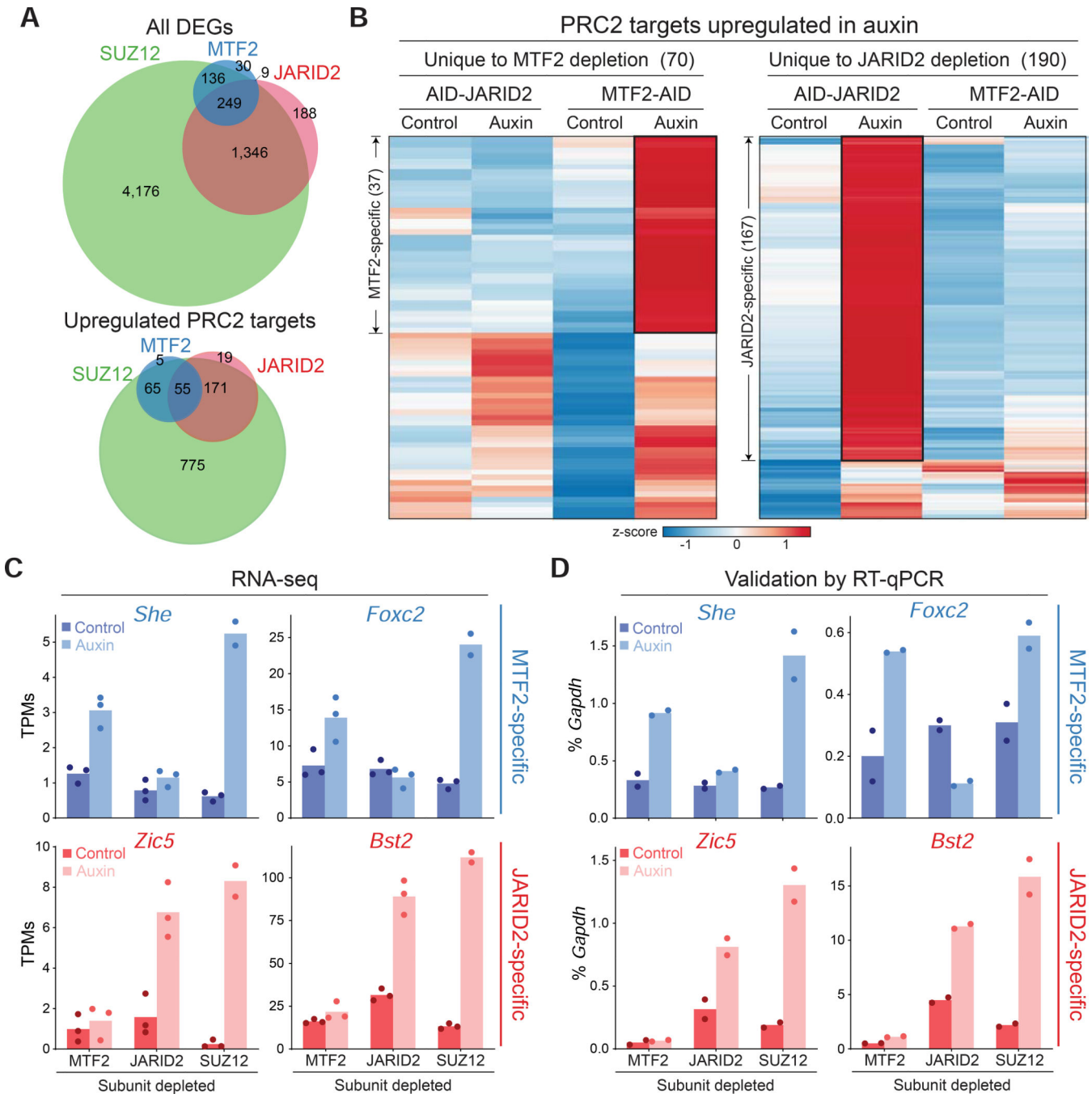

Figure 4. MTF2 and JARID2 repress distinct genes during differentiation

(A) Overlap of all differentially expressed (top) or upregulated PRC2 targets only (bottom) in SUZ12, MTF2, and JARID2 depletions at day 5 of differentiation.

(B) Heatmaps for the RNA levels of MTF2-specific (left) and JARID2-specific (right) upregulated PRC2 target genes (from 4A, bottom), at day 5 in the indicated cell lines.

(C) TPMs of representative MTF2- and JARID2-specific genes from 4B. Bars represent means; biological replicates are individual dots.

(D) Relative RNA levels (% *Gapdh)* of MTF2- and JARID2-specific genes at day 5 of differentiation. Bars represent the mean; biological replicates are individual dots. See also Figure S3B–C and Figure S4.

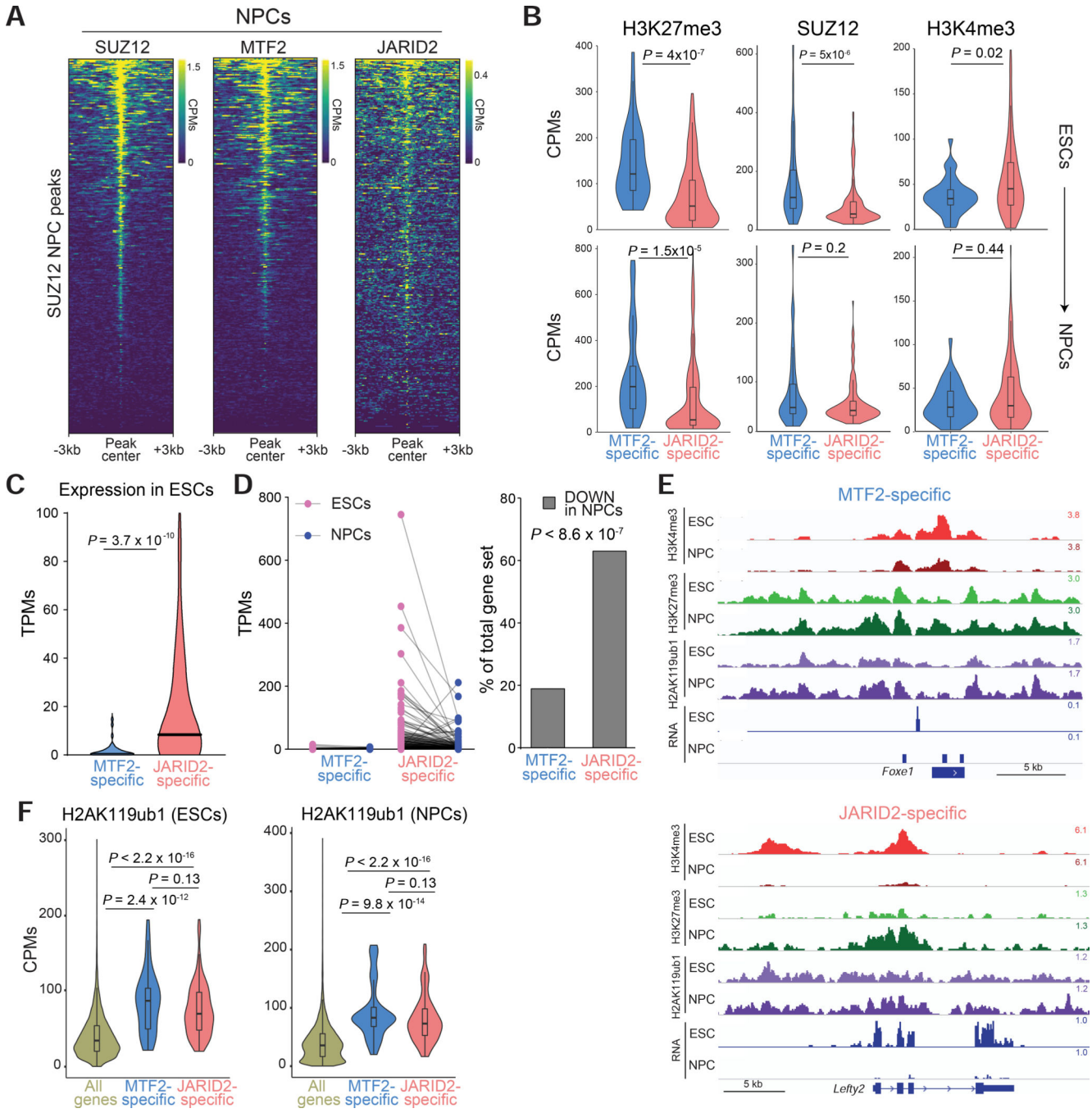

Figure 5. MTF2- and JARID2-specific genes differ in chromatin structure and expression in WT cells

(A) Heatmaps of CPMs for SUZ12, MTF2, and JARID2 from CUT&RUN in WT NPCs, centered on SUZ12 NPC peaks (n = 365) and sorted by decreasing SUZ12 signal. Data from 2 biological replicates.

(B) CUT&RUN signal (CPMs) in WT cells for H3K27me3, SUZ12, and H3K4me3 in a ± 2.5 kb region around the TSS of MTF2-specific (blue) or JARID2-specific (red) genes. *P*-values are from Mann-Whitney tests.

(C) RNA levels (TPMs) for MTF2- and JARID2-specific genes in WT ESCs. *P*-value is from Mann Whitney test.
(D) Left: RNA levels (TPMs) for MTF2- and JARID2-specific genes in WT cells before and after differentiation from ESCs to NPCs. Right: proportion of these genes that are downregulated is shown. *P*-value from Fisher's exact test.
(E) Representative genome browser tracks for H3K4me3, H3KK27me3, H2AK119ub1 and RNA levels at example MTF2- (top) or JARID2-specific (bottom) genes in WT ESCs and NPCs. The y-axis represents counts per million.
(F) CUT&RUN signal (CPMs) in WT cells for H2AK119ub1 in a ± 2.5 kb region around the TSS of all genes (mustard), MTF2-specific genes (blue), or JARID2-specific genes (red). *P*-values are from Mann-Whitney tests.
See also Figure S5 and Figure S6.

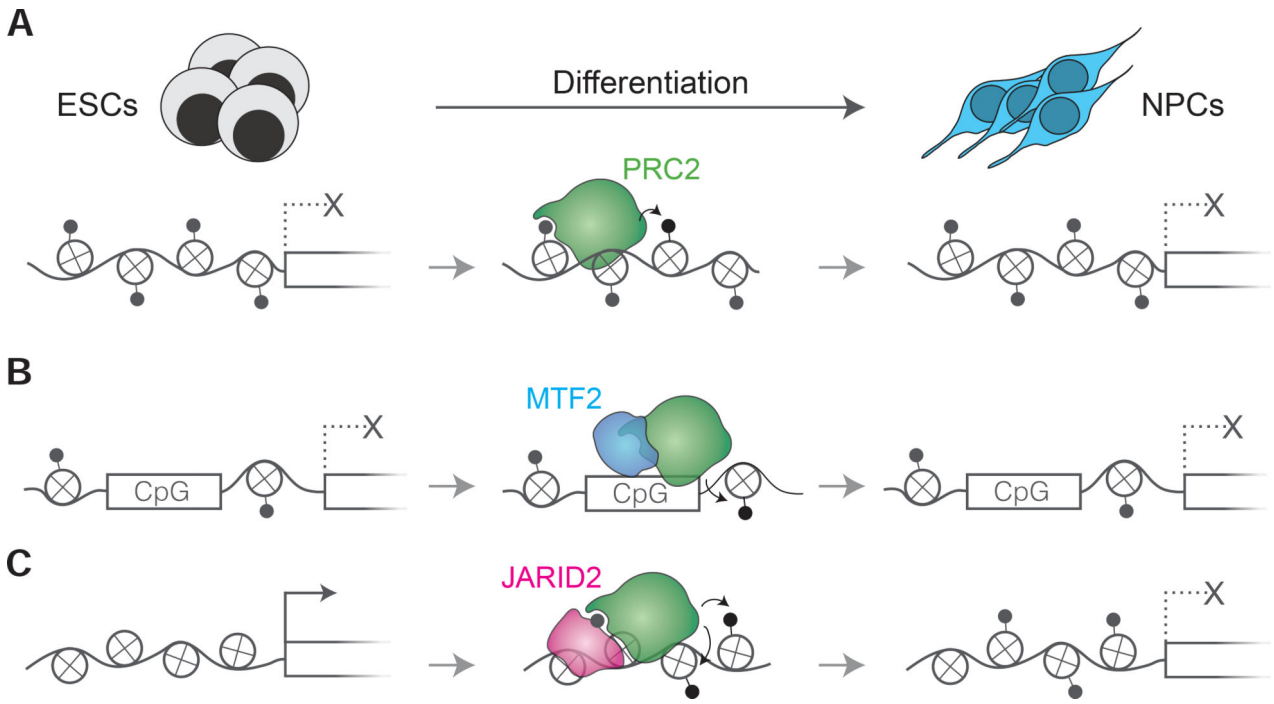

Figure 6. PRC2.1 and PRC2.2 enact different modalities of *Polycomb* repression during differentiation

(A) At a majority of target genes, PRC2.1 and PRC2.2 are redundant and H3K27me3 levels are maintained via read-write mechanisms of core PRC2 or established in an MTF2- and JARID2-independent fashion.

(B) At a subset of *Polycomb* targets with high CpG densities, high levels of H3K27me3 are not sufficient for propagation during differentiation and the function of the CpG-binding MTF2 subunit of PRC2.1 is required for silencing.

(C) Some genes that are active in ESCs and need to be newly repressed during differentiation require JARID2 to establish proper PRC2-mediated repression.

KEY RESOURCES TABLE

REAGENT or RESOURCE
Antibodies
SUZ12
EZH2
JARID2
MTF2
HA epitope
Beta-tubulin
Histone H4
GAPDH
H3K27me3 (for WB)
H3K27me3 (for CUT&RUN)
H3K4me3
H2AK119ub1
Rabbit IgG
Bacterial and Virus Strains
Biological Samples
Chemicals, Peptides, and Recombinant Proteins
Mouse bFGF
InSolution™ Smoothened Agonist, SAG - Calbiochem
Protein A MNase
Concanavalin A-coated magnetic beads
1-Thioglycerol
VEGF
Activin-A
BMP4
Human bFGF
FGF10
Indole-3-acetic acid
L-ascorbic acid
GSK-3 Inhibitor XVI (CHIR99021)
MEK1/2 Inhibitor III (PD0325901)
LIF
Critical Commercial Assays
MinElute PCR Purification kit

REAGENT or RESOURCE
Qubit dsDNA HS Assay kit
Lipofectamine 3000
Deposited Data
Raw and analyzed data
H3K27me3 in cardiac precursors
Experimental Models: Cell Lines
C57BL/6 ESCs
Experimental Models: Organisms/Strains
Oligonucleotides
Suz12 sgRNA: gCAGTGTCTGTTCAAAACATG
Mtf2 sgRNA: gTTACGTTCAGTCCTACAGTC
Jarid2 sgRNA: gTTTGGATCTCAGAATGAGCA
TIGRE locus sgRNA: gACTGCCATAACACCTAACTT
HA-AID fusion tag: GGAGGTGGTGGAAGCtacccatacgacgtgcctgactacgccggcagcggaagcGCTTGTCCTAAAGATCCAGCAAAACCCCCAGCTAAGGCTCAGGTCGTGGGATGGCCCCCTGTGA
Zic5 qPCR F: TCAAGGCCAAGTACAAGCTCA
Zic5 qPCR R: TGAAAGGCTTTTCCCCTGTAT
Bst2 qPCR F: TCCTGACAATCTACTTCGCCG
Bst2 qPCR R: CTGAAGGGTCACCACGGTC
She qPCR F: ACAGCAAGACACGGTCATCA
She qPCR R: TCCCTTTGACCTTTCGTCCG
Foxc2 qPCR F: GAAGAAGGATGTGCCCAAGGA
Foxc2 qPCR R: CCGCCTCGCTCTTAACCAC
Gapdh qPCR F: caagctcatttcctggtatgac
Gapdh qPCR R: ctcctgttattatgggggtctg
Recombinant DNA
pEN396
PX459
Software and Algorithms
STAR v2.6.1d
pheatmap (R package)
topGO (R package)
ggplot2 (R package)

Author Manuscript

Author Manuscript

Author Manuscript

REAGENT or RESOURCE
Bowtie 2 v2.3.4.3
Picard v2.19
MACS2
Repitools (R package)
Other